

¹ The effects of drought on land cover change and vegetation productivity in
² continental Chile

³ Francisco Zambrano^{a,b,*}, Anton Vrieling^c, Francisco Meza^{d,e,f}, Iongel Duran-Llacer^g, Francisco
⁴ Fernández^{h,i}, Alejandro Venegas-González, Nicolas Raab^d, Dylan Craven^{k,l}

^a Hémera Centro de Observación de la Tierra, Facultad de Ciencias, Escuela de Ingeniería en Medio Ambiente y Sustentabilidad, Universidad Mayor, Santiago, 7500994, Chile,

^b Observatorio de Sequía para la Agricultura y la Biodiversidad de Chile (ODES), Universidad Mayor, Santiago, 7500994, Chile,

^c Faculty of Geo-Information Science and Earth, University of Twente, Enschede, The Netherlands,

^d Facultad de Agronomía y Sistemas Naturales, Pontificia Universidad Católica de Chile., Santiago, Chile,

^e Instituto para el Desarrollo Sustentable. Pontificia Universidad Católica de Chile, Santiago, Chile,

^f Centro Interdisciplinario de Cambio Global, Pontificia Universidad Católica de Chile, Santiago, Chile.,

^g Hémera Centro de Observación de la Tierra, Facultad de Ciencias, Universidad Mayor,, Santiago, 7500994, Chile,

^h Center of Economics for Sustainable Development (CEDES), Faculty of Economics and Government, Universidad San Sebastian, Santiago, Chile,

ⁱ Center of Applied Ecology and Sustainability (CAPES), Santiago, Chile,

^j,

^k, GEMA Center for Genomics, Ecology & Environment, Universidad Mayor, Camino La Pirámide Huechuraba 5750, Santiago, Chile,

^lData Observatory Foundation, Santiago, Chile,

⁵ **Abstract**

Chile has experienced a persistent decrease in water supply, which impacts the hydrological system and vegetation development. This persistent period of water scarcity has been defined as a mega-drought. There are few studies about the relationship between drought and ecosystem changes that can help with a better understanding of ecological drought. The aim of our study is to evaluate the interaction of drought, land cover change, and vegetation productivity over continental Chile. To assess drought, we used drought indices for atmospheric evaporative demand (AED), water supply, and soil moisture from short- (1, 3, 6 months) to long-term (12, 24, 36 months) time scales. We derived the drought indices using monthly ERA5-Land reanalysis data from 1981 to 2023. We used the Moderate-Resolution Imaging Spectroradiometer (MODIS) datasets to derive information on annual land cover and monthly vegetation productivity. Our results showed that except for the Austral part, Chile has a temporal decreasing trend in water supply, and across the whole country, there is an increase in AED. These trends become stronger over longer time scales. We found a negative trend in vegetation productivity in the north-central area, which is more prominent for shrubland and savanna as compared to croplands and forests. The anomaly in soil moisture over the past 12 months (SSI-12) is the most important variable explaining these changes, followed by anomalies in accumulated precipitation over one to two years (SPI-12 and SPI-24). The variable importance obtained by random forest models indicates that drought is explaining about 20–30% of the change in land cover surface across Chile for forest, grassland, shrubland, and savanna but has no relation to the changes in croplands. The increase in AED is the main variable associated with the change in land cover, followed by a reduction in precipitation and soil moisture. Our findings provide insightful information that could assist in developing

adaptation measures for Chilean ecosystems to cope with climate change and drought. Also, this study could contribute to a better comprehension of ecological drought.

6 *Keywords:* drought, land cover change, vegetation productivity, ecosystem

7 **1. Introduction**

8 Drought is often classified as 1) meteorological when precipitation in a specific period remains below the
9 mean precipitation experienced in the same period during multiple years (more than 30 years usually), 2)
10 hydrological when these anomalies last for long periods (months to years) and affect water systems, and 3)
11 agricultural when the deficit negatively impacts plant health and leads to decreased productivity of crops
12 or pastures (Wilhite and Glantz, 1985). However, because drought is also influenced by human activities,
13 Van Loon et al. (2016) and AghaKouchak et al. (2021) expanded the drought definition for the Anthropocene,
14 indicating that the feedback of human decisions and activities should also be considered (i.e., anthropogenic
15 drought). Droughts lead to increased tree mortality (Cheng et al., 2024) and induces alterations in land
16 cover and land use, ultimately affecting ecosystems (Crausbay et al., 2017). Even though many ecological
17 studies have at times mistakenly considered “dry” conditions as “drought” (Slette et al., 2019). Ecological
18 drought can be defined as “*an episodic deficit in water availability that drives ecosystems beyond thresholds of
vulnerability, impacts ecosystem services, and triggers feedback in natural and/or human systems*” (Crausbay
19 et al., 2017). In light of current global warming, it is crucial to study the interaction between drought and
20 ecosystems in order to understand their feedback and impact on future water security (Bakker, 2012).

22 Global warming, as a result of human-induced greenhouse gas emissions, has increased the frequency and
23 intensity of drought, according to the sixth assessment report (AR6) of the Intergovernmental Panel on
24 Climate Change (IPCC) (Calvin et al., 2023). The evidence supporting this claim has been strengthened
25 since AR5 (IPCC, 2013). Recent studies, however, have produced contrasting findings, with some suggesting
26 that drought has not exhibited a significant trend over the past forty years (Vicente-Serrano et al., 2022;
27 Kogan et al., 2020). Vicente-Serrano et al. (2022) analyzed the trend in meteorological drought on a global
28 scale, finding that only in a few regions an increase in the severity of drought was observed. Moreover,
29 they attributed this increase solely to an increase in atmospheric evaporative demand (AED) due to higher
30 temperatures, which in turn enhances vegetation water demand, with important implications for agricultural
31 and ecological droughts. Also, they state that “*the increase in hydrological droughts has been primarily
observed in regions with high water demand and land cover change, led by an increase in agricultural land*”.
32 Similarly, Kogan et al. (2020) analyzed the drought trend using remotely-sensed vegetation health indicators,
33 finding that for the globe and main grain-producing countries, drought has not expanded or intensified during
34 the past 38 years. Nonetheless, Masson-Delmotte (2021) suggests that there is a medium to high degree
35 of confidence that rising temperatures will increase the extent, frequency, and severity of agricultural and
36 ecological droughts. Also, AR6 (Calvin et al., 2023) predicts that many regions of the world will experience
37 more severe agricultural and ecological droughts even if global warming stabilizes at 1.5°–2°C. To better
38 evaluate the impact of drought trends on ecosystems, assessments that correlate meteorological and soil
39 moisture variables to their effects on vegetation are much needed.

41 From 1960 to 2019, land use change has impacted around one-third of the Earth’s surface, which is four
42 times more than previously thought (Winkler et al., 2021). Multiple studies aim to analyze and forecast
43 changes in land cover globally (Winkler et al., 2021; Song et al., 2018) and regionally (Chamling and Bera,
44 2020; Homer et al., 2020; Yang and Huang, 2021; Schulz et al., 2010; Echeverría et al., 2012). Some seek
45 to analyze the impact of land cover change on climate conditions such as temperature and precipitation

*Corresponding author

Email addresses: francisco.zambrano@umayor.cl (Francisco Zambrano), a.vrieling@utwente.nl (Anton Vrieling), francisco.fernandez@uss.cl (Francisco Fernández)

(Luyssaert et al., 2014; Pitman et al., 2012). There is less research on drought and its relation to land cover change and vegetation productivity (Chen et al., 2022; Akinyemi, 2021; Peng et al., 2017). Peng et al. (2017) utilized net primary productivity to examine the spatial and temporal variations in vegetation productivity at global level and assess to what extent drought influenced this variability by comparing the twelve-month Standardized Precipitation Evapotranspiration Index (SPEI) and land cover change. According to their findings, drought is responsible for 37% of the decline and accounts for 55% of the variability in vegetation productivity. Chen et al. (2022) instead found poor correlations ($r<0.2$) between the vegetation productivity trends against meteorological drought (SPEI of twelve months in December) and soil moisture at the global level. These studies mostly looked at how changes in land cover and vegetation productivity are related to a single drought index (SPEI) obtained for 12 month periods. SPEI takes into account the combined effect of precipitation and AED as a water balance, but it does not allow to know the contribution of each variable on its own. To better understand these contributions on land cover change and vegetation productivity the following questions may be asked: i) how do land cover and vegetation productivity respond to short- to long-term meteorological and soil moisture droughts? And ii) How is this response different between humid and arid climatic zones? Likewise, there is a lack of understanding of how the alteration in water supply and demand is affecting land cover transformations.

To address the previous questions over extensive regions, we can utilize gridded data on water availability, vegetation conditions, and the respective drought indices. For monitoring drought, the World Meteorological Organization recommends the SPI (Standardized Precipitation Index) (WMO et al., 2012). The SPI is a multi-scalar drought index that only uses precipitation to assess short- to long-term droughts. Vicente-Serrano et al. (2010) proposed the Standardized Precipitation Evapotranspiration Index (SPEI), which incorporates the temperature effect by subtracting AED from precipitation. SPEI allows for analyzing the combined effect of precipitation and AED. Since its formulation, it has been used worldwide for the study and monitoring of drought (Gebrechorkos et al., 2023; Liu et al., 2024). Recently, there has been more interest in using AED to track droughts separately to better disengage the effects of precipitation from temperature-dependent effects (Vicente-Serrano et al., 2020). One of the reasons is that AED is linked to more flash droughts in limited water regions (Noguera et al., 2022). Hobbins et al. (2016) and McEvoy et al. (2016) developed the Evaporative Demand Drought Index (EDDI) to monitor droughts solely using the AED, and it has proven effective in monitoring flash droughts (Li et al., 2024; Ford et al., 2023). For soil moisture, several drought indices exist, such as the Soil Moisture Deficit Index (SDMI) (Narasimhan and Srinivasan, 2005) and the Soil Moisture Agricultural Drought Index (SMADI) (Souza et al., 2021). Hao and AghaKouchak (2013) and AghaKouchak (2014) proposed the Standardized Soil Moisture Index (SSI), which has a similar formulation as the SPI, SPEI, and EDDI. Thus, many drought indices exist that allow for a comprehensive assessment of drought on short- to long-term scales and that allow for the use of single variables from Earth's water balance (e.g., precipitation, AED, soil moisture). Climatic variability impacts vegetation development, with unfavorable conditions such as low precipitation and high temperatures usually promote a decrease in plant productivity. To monitor the response of vegetation for large areas, the common practice is to use satellite data. For example, the Normalized Difference Vegetation Index (NDVI) derived from frequent satellite observations of red and near infrared spectral reflectance, has been widely used as a proxy for biomass production (Camps-Valls et al., 2021; Paruelo et al., 2016; Helman et al., 2014). For Chile's cultivated land, Zambrano et al. (2018) used the zcNDVI for assessing seasonal biomass production in response to drought. Comparing the various meteo-related and vegetation-based drought indices, we can further our understanding of the impact of drought on ecosystems.

Chile's diverse climatic and ecosystem types (Beck et al., 2023; Luebert and Pliscoff, 2022) make it an ideal natural laboratory for studying climate and ecosystems. Additionally, the country has experienced severe drought conditions that have had significant effects on vegetation and water storage. North-central Chile has faced a persistent precipitation deficit since 2010, defined as a mega-drought (Garreaud et al., 2017), which has impacted the Chilean ecosystem and consequently makes it highly vulnerable to climate change (Barria et al., 2021; Alvarez-Garreton et al., 2021). This mega-drought was defined by the annual time series of the Standardized Precipitation Index (SPI) at a time scale of twelve months at the end of each year (December) when having values below one standard deviation. Some studies have addressed how this drought affects

single ecosystems in terms of forest growth ([Miranda et al., 2020](#); [Venegas-González et al., 2018](#)), forest fire occurrence ([Urrutia-Jalabert et al., 2018](#)), and crop productivity ([Zambrano, 2023b](#); [Zambrano et al., 2018, 2016](#)). The term “mega-drought” is used in Chile to describe a prolonged water shortage that lasts for several years, resulting in a permanent deficit that impacts the hydrological system ([Boisier et al., 2018](#)). Therefore, it is crucial to evaluate temporal scales that consider the cumulative impact over a period of several years. In Chile, the relationship between drought and the environment remains poorly understood. Hence, we aim to contribute to understanding how climatic and soil moisture droughts influence ecosystem dynamics in order to provide useful information that helps for a better understanding of ecological droughts and, at the same time, helps to make well-informed decisions on adaptation strategies.

Here, we analyze the multi-dimensional impacts of drought across ecosystems in continental Chile. More specifically, we aim to assess: i) short- to long-term temporal trends in multi-scalar drought indices; ii) temporal changes in land-use cover and the direction and magnitude of their relationships with trends in drought indices; and iii) the trend in vegetation productivity and its relationship with drought indices across Chilean ecosystems.

2. Study area

Continental Chile has diverse climate conditions with strong gradients from north to south and east to west ([Aceituno et al., 2021](#)) (Figure 1a), which determines its great ecosystem diversity ([Luebert and Pliscoff, 2022](#)) (Figure 1c). The Andes Mountains are a main factor in climate variation ([Garreaud, 2009](#)). For an aggregated overview of the results of the study, we used the five Chilean macrozones: “Norte Grande,” “Norte Chico,” “Centro,” “Sur,” and “Asutral”. “Norte Grande” (17°34’-25°42’S) and “Norte Chico” (25°42’-32°8’S) predominate in an arid desert climate with hot (Bwh) and cold (Bwk) temperatures. At the south of “Norte Chico,” the climate changes to an arid steppe with cold temperatures (Bsk). In these two northern regions, the land is mostly bare, with a small surface of vegetation types such as shrubland and grassland. In the macrozones “Centro” (32°08’-36°12’S) and the northern half of “Sur,” (36°12’-43°48’S) the main climate is Mediterranean, with warm to hot summers (Csa and Csb). Land cover in “Centro” comprises a significant amount of shrubland and savanna (50%), grassland (16%), forest (8%), and croplands (5%). An oceanic climate (Cfb) predominates in the south of “Sur” and the north of “Austral” (43°48’-56°00’S). Those zones have a large areal extent of forest and grassland. The southern part of the country has a tundra climate, and in “Austral,” it is a cold semi-arid area with an extended surface of grassland, forest, and, to a lesser extent, savanna.

3. Materials and Methods

3.1. Data

3.1.1. Gridded meteorological and vegetation data

To analyze land cover change, we used the classification scheme by the IGBP (International Geosphere-Biosphere Programme) from the product MCD12Q1 Collection 6.1 from MODIS. The MCD12Q1 product is produced for each year from 2001 to 2022 and defines 17 classes (see Table S1). To maintain our focus on a large scale and follow the FAO classification ([FAO, 2022](#)), we considered native and planted forests as “forests”, which represent ecosystems dominated by larger trees. To derive a proxy for vegetation productivity, we used the Normalized Difference Vegetation Index (NDVI) from the product MOD13A3 Collection 6.1 from MODIS ([Didan, 2015](#)). MOD13A3 provides vegetation indices with 1km spatial resolution and monthly frequency. The NASA EOSDIS Land Processes Distributed Active Archive Center (LP DAAC), USGS Earth Resources Observation and Science (EROS) Center, Sioux Falls, South Dakota, provided the MOD13A3 and MCD12Q1 from the online Data Pool, accessible at <https://lpdaac.usgs.gov/tools/data-pool/>.

For soil moisture, water supply, and water demand variables, we used ERA5L (ECMWF Reanalysis version 5 over land) ([Muñoz-Sabater et al., 2021](#)), a reanalysis dataset that provides the evolution of atmospheric and land variables since 1950. It has a spatial resolution of 0.1° (9 km), hourly frequency, and global coverage.

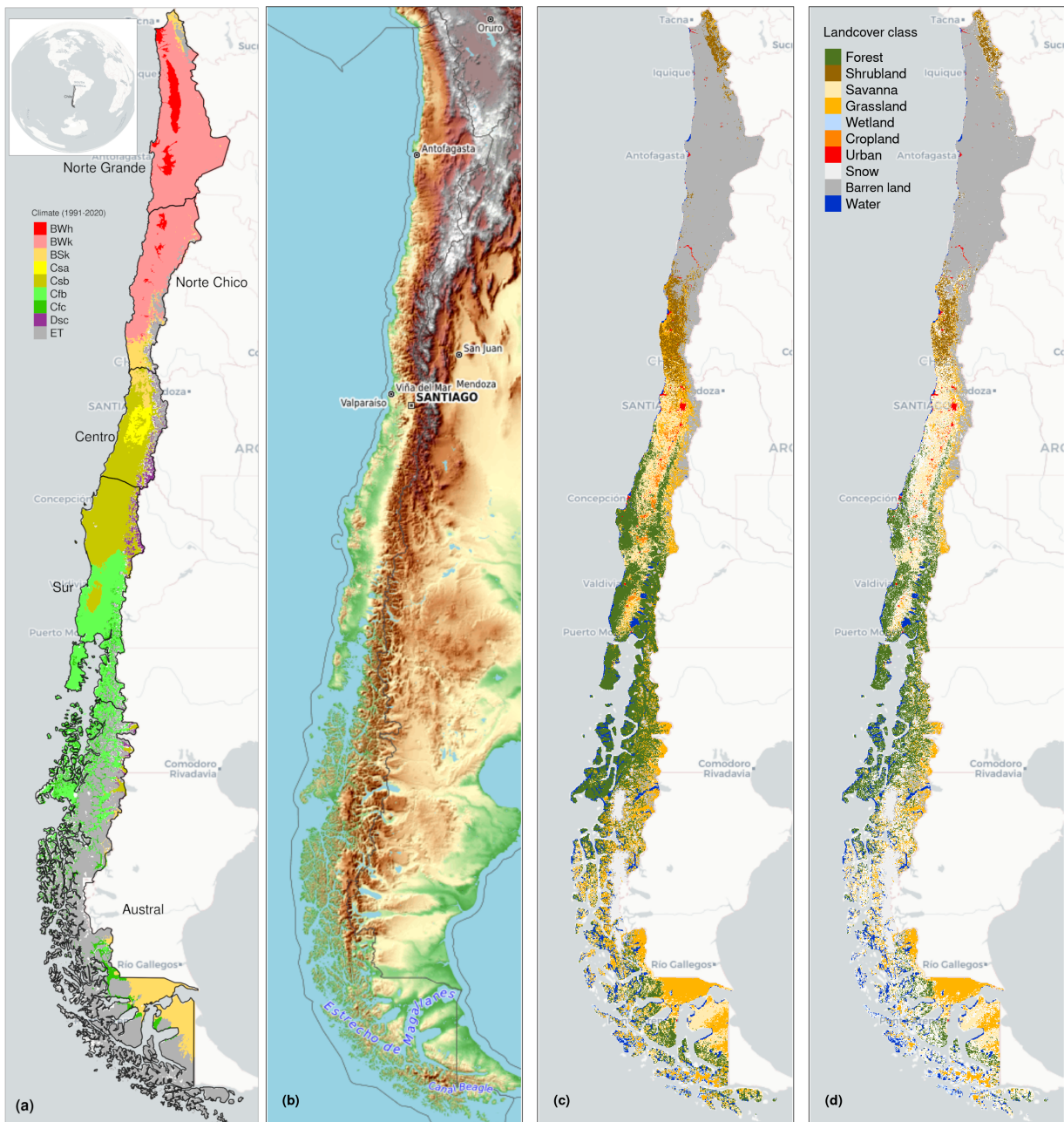


Figure 1: (a) Chile with the Koppen-Geiger climate classes and the five macrozones “Norte Grande”, “Norte Chico”, “Centro”, “Sur”, and “Austral”. (b) Topography reference map. (c) land cover classes for 2022. (d) Persistent land cover classes (> 80%) for 2001-2022

143 We selected the variables for total precipitation, maximum and minimum temperature at 2 meters, and
 144 volumetric soil water layers between 0 and 100 cm of depth (layer 1 to layer 3). 1 shows a summary of the
 145 data and its main characteristics.

Table 1: Description of the satellite and reanalysis data used

Product	Sub-product	Variable	Spatial Resolution	Period	Units	Short Name
ERA5L		Precipitation	0.1°	1981-2023	mm	P
		Maximum temperature			°C	T_{max}
		Minimum temperature			°C	T_{min}
		Volumetric Soil Water Content at 1m			m3/m3	SM
ERA5L*	MOD13A3.061	Atmospheric Evaporative Demand	0.1°	1981-2023	mm	AED
		Normalized Difference Vegetation Index			2000-2023	NDVI
MODIS	MCD12Q1.061	land cover IGBP scheme	1 km	2001-2022		land cover

*Calculated from maximum and minimum temperatures derived from ERA5L with Eq. 1.

146 *3.2. Short- to long-term drought trends*

147 *3.2.1. Atmospheric Evaporative Demand (AED)*

148 To compute the drought indices that use water demand, it is necessary to first calculate the AED. To do
149 this, we employed the Hargreaves method (Hargreaves, 1994; Hargreaves and Samani, 1985) by applying the
150 following equation:

$$AED = 0.0023 \cdot Ra \cdot (T + 17.8) \cdot (T_{max} - T_{min})^{0.5} \quad (1)$$

151 where Ra ($MJ\ m^2\ day^{-1}$) is extraterrestrial radiation; T , T_{max} , and T_{min} are mean, maximum, and
152 minimum temperature ($^{\circ}C$) at 2m. For calculating Ra we used the coordinate of the latitud of the centroid
153 of each pixel as follow:

$$Ra = \frac{14,400}{\pi} \cdot G_{sc} \cdot d_r [\omega_s \cdot \sin(\phi) \cdot \sin(\delta) + \cos(\phi) \cdot \cos(\delta) \cdot \sin(\omega_s)] \quad (2)$$

154 where

155 Ra : extraterrestrial radiation [$MJ\ m^{-2}\ day^{-1}$],

156 G_{sc} : solar constant = 0.0820 [$MJ\ m^{-2}\ min^{-1}$],

157 d_r : inverse relative distance Earth-Sun,

158 ω_s : sunset hour angle [rad],

159 ϕ : latitude [rad],

160 δ : solar declination [rad].

161 We chose the method of Hargreaves to estimate AED because of its simplicity, which only requires tem-
162 peratures and extrarrestrial radiation. Also, it has been recommended over other methods (e.g., Penman-
163 Monteith) when the access to climatic variables is limited (Vicente-Serrano et al., 2014).

164 *3.2.2. Non-parametric calculation of drought indices*

165 To derive the drought indices of water supply and demand, soil moisture, and vegetation (i.e., the proxy
166 of productivity), we used the ERA5L dataset and the MODIS product, with a monthly frequency for 1981–
167 2023 and 2000–2023, respectively. The drought indices correspond to a historical anomaly of a variable
168 (e.g., meteorological, vegetation, or soil moisture). To account for the anomaly, the common practice is to
169 derive it following a statistical parametric method in which it is assumed that the statistical distribution
170 of the data is known (Heim, 2002). A wrong decision in the statistical distribution is usually the highest
171 source of uncertainty (Laimighofer and Laaha, 2022). In the case of Chile, due to its high degree of climatic
172 variability, it is difficult to choose a proper distribution without previous research that could be applicable
173 throughout Chile. Here, we follow a non-parametric method for the calculation of the drought indices, in a
174 similar manner as the framework proposed by Farahmand and AghaKouchak (2015).

175 For the purpose of monitoring water supply drought, we used the well-known Standardized Precipitation
176 Index (SPI), which relies on precipitation data. To evaluate water demand, we chose the Evaporative
177 Demand Drought Index (EDDI), developed by Hobbins et al. (2016) and McEvoy et al. (2016), which is based

178 on the AED. The United States currently monitors drought using the EDDI (<https://psl.noaa.gov/eddi/>) as
 179 an experimental index. To consider the combined effect of water supply and demand, we selected the SPEI
 180 ([Vicente-Serrano et al., 2010](#)). For SPEI, an auxiliary variable $D = P - AED$ is calculated. Soil moisture is
 181 the main driver of vegetation productivity, particularly in semi-arid regions ([Li et al., 2022](#)). Hence, for soil
 182 water drought, we used the SSI (Standardized Soil Moisture Index) ([Hao and AghaKouchak, 2013](#)). For the
 183 SSI, we used the average soil moisture from ERA5L at 1m depth. Finally, for the proxy of productivity, we
 184 used the zcNDVI ([Zambrano et al., 2018](#)), which was derived from the monthly time series of NDVI derived
 185 from MOD13A1. All the indices are multi-scalar and can be used for the analysis of short- to long-term
 186 droughts.

187 To derive the drought indices, we first calculate the sum of the variables with regard to the time scale(s).
 188 In this case, for generalization purposes, we will use V , referring to variables P , AED , D , $NDVI$, and SM
 189 ([Table 1](#)). We accumulated each over the time series of values (months), and for the time scales s :

$$A_i^s = \sum_{i=n-s-i+2}^{n-i+1} V_i \quad \forall i \geq n-s+1 \quad (3)$$

190 The A_i^s corresponds to a moving window (convolution) that sums the variable for time scales s . Start from
 191 the last month (n) and sum the variable for s months, then follow month by month until the first month
 192 in which it could sum for s months (n-s+1). For example, using as a variable the precipitation, a period of
 193 twelve months (n), and a time scale of three months (s), it will be:

$$\begin{aligned} A_1^3 &= P_{oct} + P_{nov} + P_{dic} \\ &\vdots = \vdots + \vdots + \vdots \\ A_{10}^3 &= P_{jan} + P_{feb} + P_{mar} \end{aligned}$$

194 Then, an inverse normal approximation ([Abramowitz and Stegun, 1968](#)) obtains the empirically derived
 195 probabilities once the variable cumulates over time for the scale s . Then, we used the empirical Tukey
 196 plotting position ([Wilks, 2011](#)) over A_i to derive the $P(A_i)$ probabilities across a period of interest:

$$P(A_i^s) = \frac{i - 0.33}{n + 0.33'} \quad (4)$$

197 The drought indices SPI , $SPEI$, $EDDI$, SSI , and $zcNDVI$ are obtained following the inverse normal
 198 approximation:

$$DI(A_i^s) = W - \frac{C_0 + C_1 \cdot W + c_2 \cdot W^2}{1 + d_1 \cdot W + d_2 \cdot W^2 + d_3 \cdot W^3} \quad (5)$$

199 DI is referring to the drought index calculated for the variable V (i.e., SPI, SPEI, EDDI, SSI, and zcNDVI).
 200 The values for the constats are: $C_0 = 2.515517$, $C_1 = 0.802853$, $C_2 = 0.010328$, $d_1 = 1.432788$, $d_2 =$
 201 0.189269 , and $d_3 = 0.001308$. For $P(A_i^s) \leq 0.5$, $W = \sqrt{-2 \cdot \ln(P(A_i^s))}$, and for $P(A_i^s) > 0.5$, replace $P(A_i^s)$
 202 with $1 - P(A_i^s)$ and reverse the sign of $DI(A_i^s)$.

203 The drought indices were calculated for time scales of 1, 3, 6, 12, 24, and 36 months at a monthly frequency
 204 for 1981–2023 in order to be used for short- to long-term evaluation of drought.

205 For the proxy of vegetation productivity, we chose the time scale that best correlates with annual net
 206 primary productivity (NPP) across continental Chile. For this purpose, we calculated the zcNDVI for time
 207 scales of 1, 3, 6, and 12 months in December and compared it with the annual NPP. We used the NPP

208 from the MOD17A3HGF ([Running and Zhao, 2019](#)) dataset (MODIS). We choose to use six months because
209 the r-squared of zcNDVI with NPP highly increases from one to six months, but from six to 12 months
210 has a lower improvement. We obtained an r-squared of 0.31 for forest and 0.72 for shrubland (refer to the
211 supplementary material in Section S5). Then, we chose the proxy of vegetation productivity for six months,
212 which we will name zcNDVI hereafter. It was calculated at a monthly frequency for 2000–2023.

213 *3.2.3. Trend of drought indices*

214 To estimate if there are significant positive or negative trends for the drought indices, we used the non-
215 parametric test of Mann-Kendall ([Kendall, 1975](#)). To determine the magnitude of the trend, we used Sen's
216 slope ([Sen, 1968](#)). Some of the advantages of applying this methodology are that the Sen's slope is not
217 affected by outliers unlike regular regressions does, and it is a non-parametric method that is not influenced
218 by the distribution of the data. We applied the Mann-Kendall test to see if the trend was significant and
219 Sen's slope to estimate the magnitude of the trend. We did this for the indices SPI, EDDI, SPEI, and SSI
220 using the six time scales with data from 1981 to 2023 (monthly frequency), resulting in 24 trends (per index
221 and time scale). Then, we extracted the trend aggregated by each of the five macrozones: “Norte Grande”
222 to “Asutral,” and per land cover type: grassland, forest, cropland, shrubland, savanna, and barren land
223 (Figure 1d).

224 *3.3. Interaction of land cover and drought*

225 *3.3.1. Land cover change*

226 To analyze the land cover change, we use the IGBP scheme from the MCD12Q1 collection 6.1 from MODIS.
227 This product has been previously used for studies of drought and land cover in Chile ([Fuentes et al., 2021](#);
228 [Zambrano et al., 2018](#)). We regrouped the 17 classes into ten macroclasses, as follows: classes 1-4 to forest,
229 5-7 to shrublands, 8-9 to savannas, 10 as grasslands, 11 as wetlands, 12 and 14 to croplands, 13 as urban,
230 15 as snow and ice, 16 as barren, and 17 to water bodies. Thus, we have a land cover raster time series with
231 the ten macroclasses for 2001 and 2023. We validate the land cover macroclasses regarding a highly detailed
232 (30 m of spatial resolution) land cover map made for Chile by [Zhao et al. \(2016\)](#) for 2013-2014. Our results
233 showed a global accuracy of ~0.82 and a F1 score of ~0.66. Section S2 in the Supplementary Material shows
234 the procedure for validation.

235 We calculated the surface occupied per land cover class into the five macrozones (“Norte Grande” to
236 “Austral”) per year for 2001–2023. After that, we calculated the trend’s change in surface per land cover
237 type and macroclass. We used Mann-Kendall for the significance of the trend ([Kendall, 1975](#)) and Sen's
238 slope to calculate the magnitude ([Sen, 1968](#)).

239 To assess how water demand and supply, and soil moisture affect the variation in vegetation productivity
240 across various land cover types, we avoid analyzing areas that have major land cover changes for 2021–2022.
241 To assess how zcNDVI varied irrespective of land cover change, we developed a persistence mask for land
242 cover, which only retains pixels for which the macroclass remained the same for at least 80% of the years
243 (2001–2022) (Figure 1d).

244 *3.3.2. Relationship between land cover and drought trends*

245 The goal of this section is to identify which drought indices and time scales have a major impact on changes
246 in land cover type. We examined the relationship between the trend in land cover classes and the trend
247 in drought indices. To have more representative results, we conducted the analysis over sub-basins within
248 continental Chile. We used 469 basins, which have a surface area between 0.0746 and 24,000 km² and a
249 median area of 1,249 km². For each basin, we calculated the trend per land cover type, considering the
250 proportion of the type relative to the total surface of the basin. Then, we extracted per basin the average
251 trend (Sen's slope) of the drought indices SPI, SPEI, EDDI, SSI, and all their time scales 1, 3, 6, 12, 24,
252 and 36. Also, we extracted the average trend in the proxy of vegetation productivity (zcNDVI)

253 Random forest ([Ho, 1995](#)) employs multiple decision trees, allowing for classification and regression. Some
254 advantages include the ability to find non-linear relationships, reduce overfitting, and derive variable import-
255 tance. We used the regression random forest to model the trends in land cover per macroclass, using drought

256 indices as predictors. This included the four drought indices per six time scales and the zcNDVI, totaling
257 25 predictors. As a result, we created six random forest models, one per trend in land cover macroclass. We
258 trained 1000 forests in a resampled scheme to obtain more reliable results regarding variable importance.
259 We resampled by creating ten folds, running a random forest per fold, and calculating the r-squared (rsq),
260 root mean square error (RMSE), and variable importance. The variable importance helps for a better un-
261 derstanding of the relationships by finding which variable has a higher contribution to the model. Thus,
262 we calculate the variable's importance by permuting out-of-bag (OOB) data per tree and computing the
263 mean standard error in the OOB. After permuting each predictor variable, we repeated the process for the
264 remaining variable. We repeated this process ten times (per fold) to obtain the performance metrics (rsq,
265 RMSE, and variable importance).

266 Finally, we visually explore the connection between the SPI, EDDI, and SSI drought indices for short- and
267 long-term changes in land cover. To do this, we compare the relative changes in land cover surface (in terms
268 of the total surface area per land cover type and macrozone) with the drought indices of six (short-term) and
269 thirty-six months (long-term). We created a scatterplot in which the x-axis shows drought indices trends
270 and the y-axis shows land cover change trends.

271 3.4. Drought impacts on vegetation productivity

272 For each land cover macroclass, we analyzed the trend of vegetation productivity over the unchanged land
273 cover macroclasses. To achieve this, we used the persistent mask of land cover macroclasses , thus reducing
274 the possibility of evaluating productivity trends that are due to year-to-year variation in land cover. We
275 used the zcNDVI as a proxy of vegetation productivity. To assess productivity in Chile's cultivated land,
276 Zambrano et al. (2018) used the zcNDVI for assessing seasonal biomass production in relation to climate.

277 We examine the drought indices of water demand, water supply, and soil moisture and their correlation
278 with vegetation productivity. The objective is to determine to what extent soil moisture and water demand
279 and supply affect vegetation productivity, thus addressing three main questions: 1) Which of the drought
280 variables—supply, demand, or soil moisture—helps most in explaining the changes in vegetation productiv-
281 ity? How do the short- to long-term time scales of the drought variable affect vegetation productivity in
282 Chile? 2) How strong is the relationship between the variables and the drought index? And finally, 3) how
283 does the correlation vary per-land cover type? Answering these questions should advance our understanding
284 of how climate is affecting vegetation, considering the impact on the five land cover types: forest, cropland,
285 grassland, savanna, and shrubland.

286 We conducted an analysis on the linear correlation between the indices SPI, SPEI, EDDI, and SSI over
287 time periods of 1, 3, 6, 12, 24, and 36 months with zcNDVI. We used a method similar to that used by
288 Meroni et al. (2017) which compared the SPI time-scales with the cumulative fAPAR (fraction of Absorbed
289 Photosynthetically Active Radiation). We performed a pixel-to-pixel linear correlation analysis for each
290 index within the persistent mask of land cover macroclasses. We first compute the Pearson coefficient of
291 correlation for each of the six time scales. A time scale is identified as the one that attains the highest
292 correlation ($p < 0.05$). We then extracted the Pearson correlation coefficient corresponding to the time
293 scales where the value peaked. As a result, for each index, we generated two raster maps: 1) containing
294 the raster with values of the time scales and drought index that reached the maximum correlation, and 2)
295 having the magnitude of the correlation obtained by the drought index at the time scales.

296 3.5. Software

297 For the downloading, processing, and analysis of the spatio-temporal data, we used the open source software
298 for statistical computing and graphics, R (R Core Team, 2023). For downloading ERA5L, we used the
299 {ecmwfr} package (Hufkens et al., 2019). For processing raster data, we used {terra} (Hijmans, 2023) and
300 {stars} (Pebesma and Bivand, 2023). For managing vectorial data, we used {sf} (Pebesma, 2018). For
301 the calculation of AED, we used {SPEI} (Beguería and Vicente-Serrano, 2023). For mapping, we use {tmap}
302 (Tennekes, 2018). For data analysis and visualization, the suite {tidyverse} (Wickham et al., 2019) was used.
303 For the random forest modeling, we used the {tidymodels}(Kuhn and Wickham, 2020) and {ranger}(Wright
304 and Ziegler, 2017) packages.

305 **4. Results**

306 *4.1. Short- to long-term drought trends*

307 Figure 2 shows the spatial variation of the trend for the drought indices from short- to long-term scales.
308 The white space on the maps indicates a not significant trend. SPI and SPEI have a decreasing trend
309 from “Norte Chico” to “Sur.” However, there is an increasing trend in “Austral.” The degree of the trend
310 is stronger at higher time scales. The SSI indicates that in “Norte Grande,” there are surfaces that have
311 increased in the southwest and in the northeast have decreased, and are shown for all time scales. Similar
312 to SPI and SPEI, SSI decreases at higher time scales. EDDI showed a positive trend for the whole of
313 continental Chile, with a higher trend toward the north and a descending gradient toward the south. The
314 degree of trend increases at higher time scales.

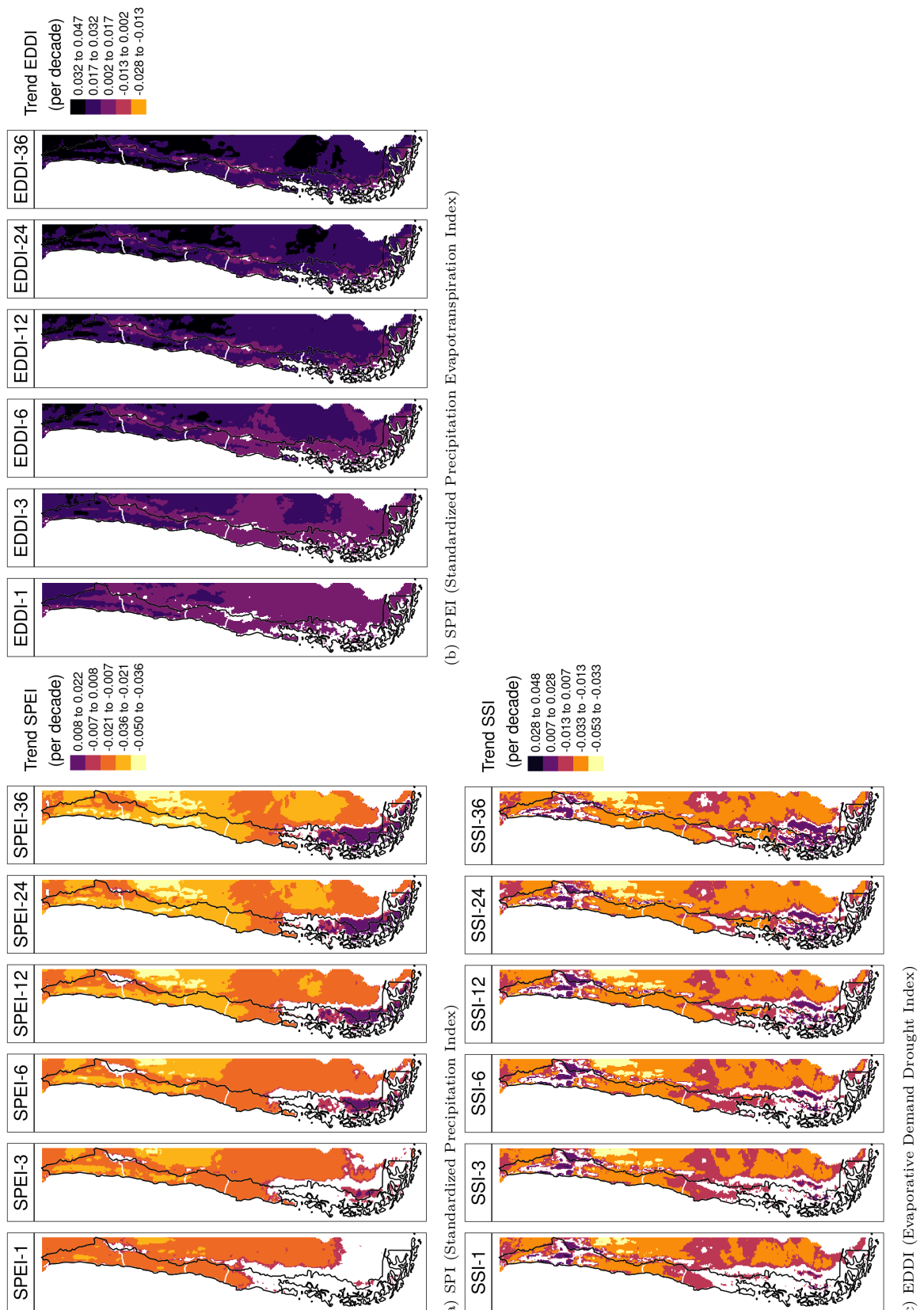


Figure 2: Linear trend of the drought index (*) at time scales of 1, 3, 6, 12, 24, and 36 months for 1981-2023

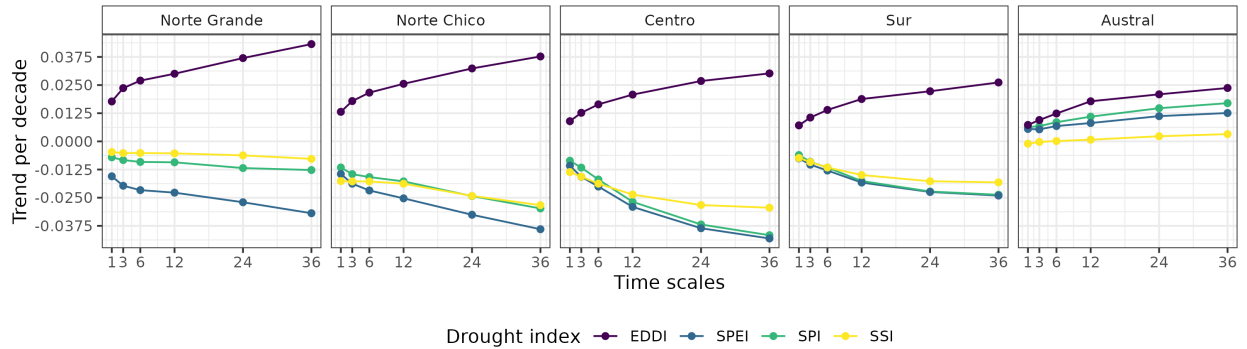


Figure 3: Trend per decade for the drought indices SPI, EDDI, SPEI, and SSI aggregated by macrozone.

315 The Figure 3 displays the averaged aggregation per macrozone, the drought index, and the timescale. The
 316 macrozones that reached the lowest trend for SPI, SPEI, and SSI are “Norte Chico” and “Centro,” where
 317 the indices also decrease at longer time scales. This may potentially be explained by the prolonged reduction
 318 in precipitation that has affected the hydrological system in Chile. At 36 months, it reaches trends between
 319 -0.03 and -0.04 (z-score) per decade for SPI, SPEI, and SSI. For “Sur,” the behavior is similar, decreasing
 320 at longer scales and having between -0.016 and -0.025 per decade for SPI, SPEI, and SSI. “Norte Grande”
 321 has the highest trend at 36 months for EDDI (0.042 per decade), and “Centro” has the lowest for SPI and
 322 SPEI. In “Norte Grande” and “Norte Chico,” which are in a semi-arid climate, it is evident that the EDDI
 323 has an effect on the difference between the SPI and SPEI index, which is not seen in the other macrozones.
 324 Contrary to the other macrozones, “Austral” showed an increase in all indices, being the highest for EDDI
 325 at 36 months (0.025) and the lowest for SSI, which shows only a minor increase in the trend.

326 4.2. Interaction of land cover and drought

327 4.2.1. Land cover change

Table 2: Surface per land cover class that persists during 2001–2022.

Macrozone	Surface [km ²]					
	Forest	Cropland	Grassland	Savanna	Shrubland	Barren land
Norte Grande		886		7,910	171,720	
Norte Chico	90	4,283	589	16,321	84,274	
Centro	3,739	1,904	7,584	19,705	844	12,484
Sur	72,995	1,151	7,198	15,906		2,175
Austral	60,351		54,297	19,007	249	7,218
Total	137,085	3,145	74,247	55,206	25,324	277,870

328 For vegetation, we obtained and used hereafter five macroclasses of land cover from IGBP MODIS: forest,
 329 shrubland, savanna, grassland, and croplands. Figure 1c shows the spatial distribution of the macroclasses
 330 through Chile for the year 2022. Figure 1d shows the macroclasses of land cover persistence (80%) during
 331 2021–2022, respectively (Table 2). Within continental Chile, barren land is the land cover class with the
 332 highest surface area ($277,870 \text{ km}^2$). The largest type of vegetation, with $137,085 \text{ km}^2$, is forest. Grassland
 333 has $74,247 \text{ km}^2$, savanna $55,206 \text{ km}^2$, shrubland $25,324 \text{ km}^2$, and cropland $3,146 \text{ km}^2$ (Table 2). The
 334 macrozones with major changes for 2001–2022 were “Centro,” “Sur,” and “Austral,” with 36%, 31%, and
 335 34% of their surface changing the type of land cover, respectively (Figure 1 and Table 3). Figure 4 shows
 336 the summary of the proportion of surface per land cover class and macrozone, derived from the persistence
 337 mask over continental Chile.

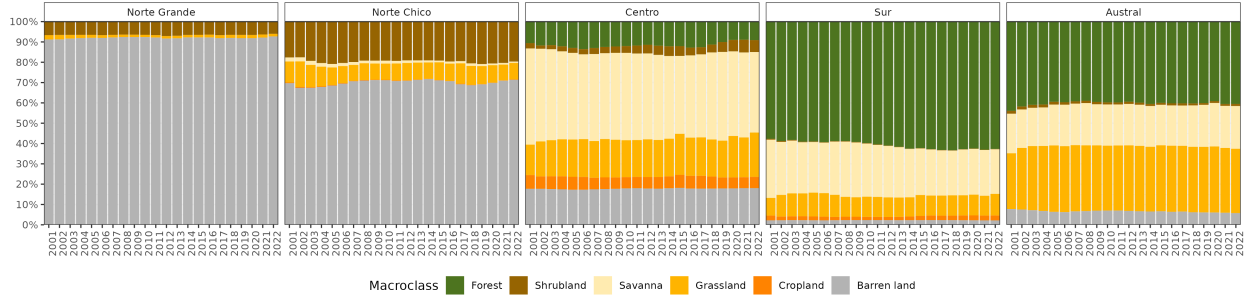


Figure 4: Proportion of land cover class from the persistent land cover for 2001–2022 (>80%) per macrozone and land cover macroclass.

Table 3: The value of Sen's slope trend next to the time-series plot of surface per land cover class (IGBP MCD12Q1.016) for 2001–2022 through Central Chile. Values of zero indicate that there was not a significant trend. The red dots on the plots indicate the maximum and minimum values of the surface. Cells without values indicate that the land cover type was not significant in that macrozone.

Trend of change [$\text{km}^2 \text{ year}^{-1}$]						
Macrozone	Forest	Cropland	Grassland	Savanna	Shrubland	Barren land
Norte Grande				0		0
Norte Chico		-12	0	-70	0	111
Centro	0	-22	83	-136	146	23
Sur	397	38	0	-319		0
Austral	0		0	172	-37	-93

338 From the trend analysis in Table 3, we can indicate that the “Norte Chico” shows an increase in barren
 339 land of $111 \text{ km}^2 \text{ yr}^{-1}$ and a reduction in the class savanna of $70 \text{ km}^2 \text{ yr}^{-1}$. In the “Centro” and “Sur,” there
 340 are changes with an important reduction in savanna with 136 and $319 \text{ km}^2 \text{ yr}^{-1}$, respectively, and an increase
 341 in shrubland and grassland, showing a change for more dense vegetation types. The area under cultivation
 342 (croplands) appears to be shifting from the “Centro” to the “Sur.” Also, there is a high increase in forest
 343 ($397 \text{ km}^2 \text{ yr}^{-1}$) in the “Sur,” seemingly replacing the savanna lost (Table 3).

344 4.2.2. Relationship between drought indices and land cover change

345 The random forest models for estimating the land cover trend based on the trends in drought indices reach
 346 an R^2 between 0.32 and 0.39 for the land cover types (Table 4) excluding cropland. It is more likely that
 347 short- and medium-term increases in AED (EDDI-6 and EDDI-12) and short-term precipitation deficits
 348 (SPI-6 and SPEI-6) are associated to changes in grassland and bare land. The short-term increase of AED
 349 (EDDI-3 and EDDI-6) and the longer duration of the precipitation deficit (SPI-24, SPI-36, and SPEI-36)
 350 were the most important variables that correlated with changes in shrubland. The changes in savanna are
 351 associated with a short- and long-term increase in AED and a three-year precipitation deficit (SPI-36). The
 352 increase in cumulative AED from 12 to 36 months is the strongest associated variable that contributes to
 353 changes in forests, followed by the reduction of soil moisture over six and 36 months. The supplementary
 354 material in Section S3 provides further details about the variable’s importance.

355 Figure 6 shows the connection between the SPI, EDDI, and SSI drought indices and changes in land cover.
 356 Forest in the “Sur,” shrubland and grassland in “Centro,” barren land in “Norte Chico,” and savanna in
 357 “Austral” showed an increase in land cover extent, which was associated with an increase in EDDI. Savanna
 358 in “Centro,” “Sur,” and “Norte Chico” decreases with the increase in EDDI. The SPI and SSI showed similar
 359 behavior regarding the trend in land cover type. A decrease in SPI and SSI is associated with an increase

Table 4: The five most important trends of drought indices in estimating the landcover trend per land cover type and the r-squared (rsq) reached by each random forest model.

Macrozone	Forest	Cropland	Grassland	Savanna	Shrubland	Barren Land
Norte Grande	EDDI-36	SPI-24	SPEI-36	SPI-36	SPI-36	EDDI-6
Norte Chico	EDDI-3	SPI-24	SPEI-36	EDDI-12	SPI-36	EDDI-6
Centro	SPEI-36	SPI-24	EDDI-6	SPI-36	SPI-36	EDDI-6
Sur	EDDI-36	SPI-24	SPEI-36	EDDI-36	SPI-36	SPEI-24
Austral	EDDI-36	SPI-24	EDDI-6	SPI-36	SPI-36	SPEI-24



360 in the surface in shrubland and grassland in “Centro,” forest in “Sur,” and barren land in “Norte Chico,”
 361 as well as a decrease trend in savanna in “Norte Chico,” “Centro,” and “Sur.”

362 *4.3. Drought impacts on vegetation productivity within land cover*

363 *4.3.1. Trends in vegetation productivity*

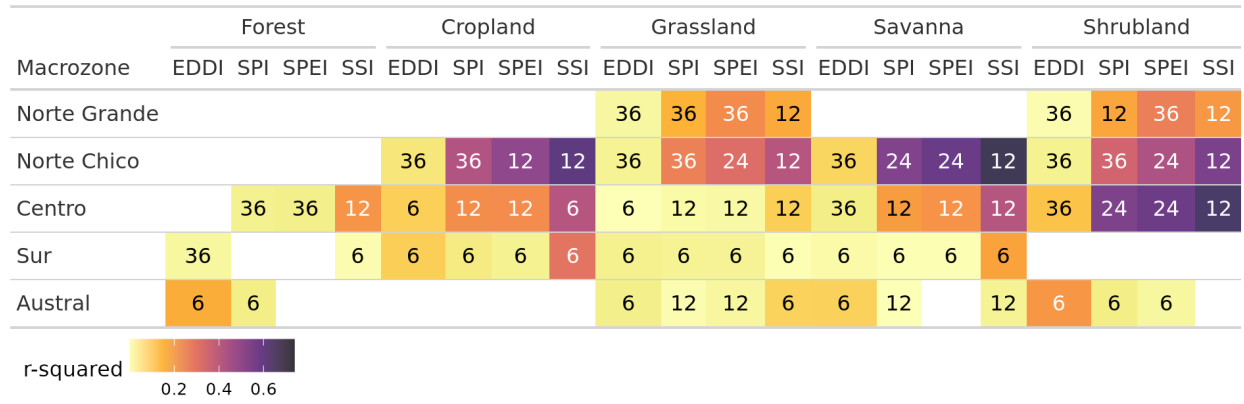
364 The temporal variation within the macrozones is shown in Figure 7b. There is a negative trend in “Norte
 365 Chico” with -0.035 and “Centro” with -0.02 per decade. Vegetation reached its lowest values for 2019-2022,
 366 with an extreme condition in early 2020 and 2022 in the “Norte Chico” and “Centro”. The “Sur” and
 367 “Austral” show a positive trend of around 0.012 and 0.016, respectively, per decade (Figure 7).

368 In Figure 7 it is showed the spatial map of trends in zcNDVI (Figure 7a). In “Norte Grande,” vegetation
 369 productivity, as per the z-index, exhibits a yearly increase of 0.027 for grassland and 0.032 for shrubland. In
 370 the “Norte Chico,” savanna has the lowest trend of -0.062, cropland -0.047, shrubland -0.042, and grassland
 371 -0.037. In “Centro,” shrubland reaches -0.07, savanna -0.031, cropland -0.024, forest -0.017, and grassland
 372 -0.005 per decade. This decrease in productivity could be associated either with a reduction in vegetation
 373 surface, a decrease in biomass, or browning.

374 4.3.2. Correlation between vegetation productivity and drought indices

375 Figure 8 shows the highest coefficient of determination (r^2 , or rsq) found in the regression analysis
 376 between zcNDVI and different drought indicators over time scales of 1, 3, 6, 12, 24, and 36 months. The
 377 spatial variation of time scales reached per index is mostly for time scales above 12 months. In the case of
 378 SSI, the predominant scales are 6 and 12 months. For all indices, to the north, the time scales are higher
 379 and diminish toward the south until the south part of “Austral,” where they increase. In Figure 9, the map
 380 of Pearson correlation values (r) is shown. The EDDI reached correlations above 0.5 between “Norte Chico”
 381 and “Sur.” The correlation changes from negative to positive toward the Andes Mountains and to the sea,
 382 just as in the northern part of “Austral.” The SPI and SPEI have similar results, with the higher values in
 383 “Norte Chico” and “Centro” being higher than 0.6. Following a similar spatial pattern as EDDI but with an
 384 opposite sign. The SSI showed to be the index that has a major spatial extension with a higher correlation.
 385 It has a similar correlation to SPI and SPEI for “Norte Chico” and “Sur,” but has improvements for “Sur.”

Table 5: Summary per land cover macroclass and macrozone regarding the correlation between zcNDVI with the drought indices EDDI, SPI, SPEI, and SSI for time scales of 1, 3, 6, 12, 24, and 36. The numbers in each cell indicate the time scale that reached the maximum correlation for the land cover and macrozone, and the color indicates the strength of the r^2 obtained with the index and the time scale. Cells without values indicate that the land cover type was not significant in that macrozone.



386 In Table 5, we aggregate per macrozone and land cover the correlation analysis presented in Figure 8 and
 387 Figure 9. According to what is shown, forests seem to be the most resistant to drought. Showing that
 388 only “Centro” is slightly ($r^2 = 0.25$) impacted by a 12-month soil moisture deficit (SSI-12). In the “Norte
 389 Chico” and to a lesser extent in the “Norte Grande,” it is evident that a SSI-12 with a $r^2 = 0.45$ and a
 390 decrease in water supply (SPI-36 and SPEI-24 with $r^2 = 0.28$ and 0.34, respectively) have an impact on
 391 grasslands. However, this type was unaffected by soil moisture, water supply, or demand in macrozones
 392 further south. The types that show to be most affected by variation in climate conditions are shrublands,
 393 savannas, and croplands. For savannas in “Norte Chico,” the SSI-12 and SPI-24 reached an r^2 of 0.74
 394 and 0.58, respectively. This value decreases to the south, but the SSI-12 is still the variable explaining
 395 more of the variation in vegetation productivity ($r^2 = 0.45$ in “Centro” and 0.2 in “Sur”). In the case
 396 of croplands, the SPEI-12, SPI-36, and SSI-12 explain between 45% and 66% of the variability in “Norte
 397 Chico.” The type of land most impacted by climatic variation was shrubland, where soil moisture explained
 398 59% and precipitation, 37%, in “Norte Chico” and “Centro,” with SSI-12 being the most relevant variable,
 399 then SPI-36 in “Norte Chico” and SPI-24 in “Sur.”

400 5. Discussion

401 5.1. Vegetation water demand and its relation to drought

402 In our study, we took into account the variation in vegetation productivity in Chile, specifically in areas
 403 without any changes in land cover, to prevent any misleading conclusions about the increase in water demand

404 due to land cover change. Our results show a contrasting perspective regarding the evidence provided by
405 [Vicente-Serrano et al. \(2022\)](#) on a global scale, who indicates that the increase in drought is led by an
406 increase in agricultural land, which in turn increases water demand.

407 Our results indicate that except for the southern part of the country, the SPI, SPEI, and SSI (water supply)
408 showed declining trends, while the EDDI (water demand) increased across continental Chile. The trends
409 in water demand and supply were stronger as the time scales increased, indicating a long-term reduction
410 in water supply (except for the southern part) and an increase in water demand by the atmosphere. Also,
411 we found that there has been a significant declining trend in vegetation productivity (zcNDVI) since 2000
412 for the north-central part of the country, which reached its lowest level between 2020 and 2022 and has
413 impacted natural and cultivated land. Further, croplands showed a decrease in surface area for the north-
414 central region, while barren land increased. We link these changes to a decrease in the water demand
415 from vegetation because, despite the increase in AED, the surface area for water-demanding vegetation is
416 declining as well as the biomass production. However, some questions arise regarding what is occurring with
417 the cultivated land. Evidence suggests that higher-water-demanding crops have replaced croplands in the
418 Petorca basin (central Chile), leading to an increase in water abstraction ([Muñoz et al., 2020](#); [Duran-Llacer
419 et al., 2020](#)). Nonetheless, at this scale of analysis, the effect of higher crop water demand on drought is
420 minor compared to the decrease in water supply and increase in AED over all land cover types.

421 The long-scale trends (e.g., 36 months) demonstrate the impact of human-induced climate change on
422 water availability in Chile, potentially due to an intense hydrological drought stemming from the ongoing
423 precipitation deficit and rising AED. But it is likely that in zones most affected by drought, the main cause
424 is not an increase in vegetation water demand due to an intensification of cultivated land (e.g., an increase
425 in irrigated crops) like in other parts of the globe ([Vicente-Serrano et al., 2020](#)). North-central Chile has
426 experienced a decline in vegetation productivity across land cover types, which is primarily attributable to
427 variations in water supply and soil moisture. An increase in water demand, led by an increase in the surface
428 area of irrigated crops or the change to more water-demanding crops, could strengthen this trend, however,
429 it escapes the scope of this study. Future work should focus on the regions where the drought has been
430 more severe and has a high proportion of irrigated crops to get insight on the real impact of irrigation on
431 ecosystems in those zones.

432 *5.2. Sensitivity of land cover vegetation to short- and long-term drought*

433 We analyzed the time series of drought indices and vegetation productivity per land cover type. Our results
434 indicate that forest is the type most resistant to drought, and shrublands, savannas, and croplands have
435 higher sensitivity.

436 In their study in the Yangtze River Basin in China, [Jiang et al. \(2020\)](#) analyzed the impact of drought on
437 vegetation using the SPEI and the Enhanced Vegetation Index (EVI). They found that cropland was more
438 sensitive to drought than grassland, showing that cropland responds strongly to short- and medium-term
439 drought (< SPEI-6). In our case, the SPEI-12 was the one that most impacted the croplands in “Norte
440 Chico” and “Centro.” In general, most studies show that croplands are most sensitive to short-term drought
441 (< SPI-6) ([Zambrano et al., 2016](#); [Potopová et al., 2015](#); [Dai et al., 2020](#); [Rhee et al., 2010](#)). Short-term
442 precipitation deficits have an impact on soil water, so less water is available for plant growth. However, we
443 found that in “Norte Chico,” an SPI-36 and SPEI-12 had a higher impact, which are associated with long-
444 term water deficit, and in “Centro,” an SPI-12 and SPEI-12. Thus, we hypothesize that this impact could
445 be attributed to the hydrological drought that has decreased groundwater storage ([Tau care et al., 2024](#)),
446 which in turn is impacted by long-term deficits, and consequently, the vegetation is more dependent on
447 groundwater. In “Sur” and “Austral,” the correlations between drought indices and vegetation productivity
448 decrease, as do the time scales that reach the maximum r-squared. The possible reason for this is that the
449 most resistant types, forest and grassland, predominate south of “Centro.” Also, drought episodes have been
450 less frequent and intense and have had a lower impact on water availability for vegetation.

451 According to [Senf et al. \(2020\)](#), severe drought conditions in Europe are a significant cause of tree mortality.
452 However, we discovered that forests are the most resilient land cover class to drought, with less variation

453 in drought indices. Supporting this is Fathi-Taperasht et al. (2022), who assert that Indian forests are
454 the most drought-resistant and recover rapidly. Similarly, the work of Wu et al. (2024), who analyzed
455 vegetation loss and recovery in response to meteorological drought in the humid subtropical Pearl River
456 basin in China, indicates that forests showed higher drought resistance. Using Vegetation Optical Depth
457 (VOD), kNDVI, and EVI, Xiao et al. (2023) tested the resistance of ecosystems and found that ecosystems
458 with more forests are better able to handle severe droughts than croplands. They attribute the difference to
459 a deeper rooting depth for trees, a higher water storage capacity, and different water use strategies between
460 forest and cropland (Xiao et al., 2023).

461 In central Chile, Venegas-González et al. (2023) observed a significant decline in the overall growth of
462 sclerophyllous moist forests (mediterranean forests), which they attributed to increased drought conditions.
463 In another study, Fuentes et al. (2021) evaluated water scarcity and land cover change in Chile between 29°
464 and 39° south latitude. They used the one-month SPEI for drought evaluation, which resulted in misleading
465 results. For instance, they failed to identify a temporal trend in the SPEI, but they still observed a decline
466 in water availability and a rise in AED, trends that should have been detectable if they were using longer
467 SPEI time scales. Thus, according to the results presented in this study, for the assessment of drought, it is
468 necessary to consider drought indices on a short- to long-scale basis.

469 5.3. Vegetation productivity and drought

470 We found that the 12-month soil moisture deficit affected plant productivity in all land cover types in
471 Chile. The main external factors that affect biomass production by vegetation are actual evapotranspiration
472 and soil moisture, and the rate of ET in turn depends on the availability of water storage in the root zone.
473 Thus, soil moisture plays a key role in land carbon uptake and, consequently, in the production of biomass
474 (Humphrey et al., 2021). The study results showed that the soil moisture-based drought index (SSI) was
475 better at explaining vegetation productivity across land cover macroclasses than meteorological drought
476 indices like SPI, SPEI, and EDDI. According to (Chatterjee et al., 2022) in the early growing season and
477 especially in irrigated rather than rainfed croplands, soil moisture has better skills than SPI and SPEI for
478 estimating gross primary production (GPP) . Also, Zhou et al. (2021) indicate that the monthly scaled
479 Standardized Water Deficit Index (SWDI) can accurately show the effects of agricultural drought in most
480 of China. Nicolai-Shaw et al. (2017) also looked at the time-lag between the SWDI and the Vegetation
481 Condition Index (VCI). They found that there was little to no time-lag in croplands but a greater time-lag
482 in forests.

483 In our case, there is strong spatial variability throughout Chile and between classes, mainly attributable to
484 climate heterogeneity, hydrological status, or vegetation resistance to water scarcity. The semi-arid “Norte
485 Chico” and the Mediterranean “Centro” were where SSI had the best performance. In Chile, medium-
486 term deficits of 12 months are more relevant in the response of vegetation for all land cover types, which
487 decreases to the south, and in the case of croplands, they seem to react in a shorter time, with six months
488 (SSI-6) in “Centro.” This variation for croplands could be related to the fact that in “Norte Chico,” the
489 majority of crops are irrigated, but to the south there is a higher proportion of rainfed agriculture, which
490 is most dependent on the short-term availability of water. Rather, in “Norte Chico,” the orchards are more
491 dependent on irrigation, which in turn depends on the availability of storage water in dams of groundwater
492 reservoirs, which are affected by long-term drought (e.g., SPI-36).

493 5.4. Drought information to aid in adaptation

494 Our findings present valuable information for policymakers in developing adaptation strategies for droughts.
495 Our results show that the different climate components, such as AED, water supply, soil moisture, and their
496 impact on vegetation, should be considered when evaluating the multi-dimensional nature of drought. Also,
497 for a better understanding of drought propagation (Van Loon et al., 2012) from meteorological to agricultural
498 and ecological drought, we should consider the climatic response at different time scales, ranging from short
499 to long. Additionally, the spatiotemporal characteristics of our results allow us to distinguish distinct
500 geographical contexts, recognizing the diversity in climate, but also shedding light on agricultural practices

501 (ranging from irrigated to dryland farming), technological advancements in irrigation efficiency, and the
502 region-specific capabilities for drought adaptation, including groundwater management and reservoir water
503 storage. This information, combined with agricultural information and statistics, could provide a strong
504 foundation for the development of science-based adaptation policies.

505 In a commitment to fostering informed and dynamic adaptation efforts, our results are disseminated
506 publicly and continually updated via the Drought Observatory for Agriculture and Biodiversity of Chile
507 (ODES) (<https://odes-chile.org/app/unidades>) (Zambrano, 2023a; Kunst and Zambrano, 2023). This ini-
508 tiative ensures the availability of extensive climate data, facilitating the development of adaptive strate-
509 gies that are both responsive to the realities of different regions and grounded in the latest scientific
510 understanding. The proactive sharing and updating of such data underscores its key role in enabling
511 policymakers to craft adaptive measures that are finely tuned to the diverse and evolving landscapes
512 of drought impacts. Furthermore, the recently promulgated law about climate change in Chile (Law
513 21.455, <https://www.bcn.cl/leychile/navegar?idNorma=1177286>), which aims to implement sectoral adap-
514 tation plans for agriculture, forests, and biodiversity, could benefit from this information.

515 6. Conclusion

516 We found a significant trend toward decreasing water supply (SPI, SPEI, and SSI) in most of the Chilean
517 territory, with the exception of the southern region. The trend is the strongest in the north-central zone. The
518 whole country showed an increase in water demand (AED) due to increasing temperatures. The magnitude
519 of the trends is stronger for longer time scales, which is evidence that there is a prolonged precipitation
520 shortage and a prolonged increase in AED. The trend in vegetation productivity in the north-central area
521 is affecting shrubland and savanna to a greater degree, followed by croplands and forests.

522 We model about 20–30% of the trends in land cover types, such as forest, grassland, shrubland, and savanna,
523 based on drought indicators across Chile. There is no evidence that drought alters cropland surface area.
524 The increase in AED is the most important variable explaining the variability in the change in land cover,
525 followed by a reduction in precipitation and soil moisture.

526 The trends in drought indices are accompanied by multiple land cover changes in the country, most notably
527 an increase of forest in “Sur,” of shrubland and grassland in “Centro,” and of savanna in “Centro” and “Sur.”
528 In “Norte Chico” and “Centro,” the croplands have been declining in surface, whereas in “Sur,” there is an
529 increase in cultivated land.

530 The change in vegetation productivity has been severe in the north-central part of the country for all land
531 cover types, particularly savanna, shrubland, and croplands. The anomaly in soil moisture over the past
532 12 months is the main variable explaining these changes, followed by anomalies in accumulated precipita-
533 tion over one to two years. The variation in AED seems to intensify the drought impact on vegetation
534 productivity.

535 The results of this study provide insightful information that would assist in developing adaptation measures
536 for Chilean ecosystems to cope with climate change and drought. Information that could be used in the
537 scope of the national law on climate change, which seeks to implement adaptation strategies for agriculture,
538 forests, and biodiversity.

539 7. Acknowledgment

540 The National Research and Development Agency of Chile (ANID) funded this study through the drought
541 emergency project FSEQ210022, Fondecyt Iniciación N°11190360, Fondecyt Postdoctorado N°3230678, and
542 Fondecyt Regular N°1210526.

- 543 **References**
- 544 Abramowitz, M., Stegun, I.A., 1968. Handbook of mathematical functions with formulas, graphs, and mathematical tables. volume 55. US Government printing office.
- 545 Aceituno, P., Boisier, J.P., Garreaud, R., Rondanelli, R., Rutllant, J.A., 2021. Climate and Weather in Chile, in: Fernández, B., Gironás, J. (Eds.), Water Resources of Chile. Springer International Publishing, Cham. volume 8, pp. 7–29. URL: http://link.springer.com/10.1007/978-3-030-56901-3_2.
- 546 Aghakouchak, A., 2014. A baseline probabilistic drought forecasting framework using standardized soil moisture index: application to the 2012 United States drought. *Hydrology and Earth System Sciences* 18, 2485–2492. URL: <https://hess.copernicus.org/articles/18/2485/2014/>, doi:10.5194/hess-18-2485-2014.
- 547 Aghakouchak, A., Mirchi, A., Madani, K., Di Baldassarre, G., Nazemi, A., Alborzi, A., Anjileli, H., Azarderakhsh, M., Chiang, F., Hassanzadeh, E., Huning, L.S., Mallakpour, I., Martinez, A., Mazdiyasni, O., Moftakhari, H., Norouzi, H., Sadegh, M., Sadeqi, D., Van Loon, A.F., Wanders, N., 2021. Anthropogenic Drought: Definition, Challenges, and Opportunities. *Reviews of Geophysics* 59, e2019RG000683. URL: <https://agupubs.onlinelibrary.wiley.com/doi/10.1029/2019RG000683>, doi:10.1029/2019RG000683.
- 548 Akinyemi, F.O., 2021. Vegetation Trends, Drought Severity and Land Use-Land Cover Change during the Growing Season in Semi-Arid Contexts. *Remote Sensing* 2021, Vol. 13, Page 836 13, 836. URL: <https://www.mdpi.com/2072-4292/13/5/836/htm>, doi:10.3390/RS13050836. publisher: Multidisciplinary Digital Publishing Institute.
- 549 Alvarez-Garreton, C., Boisier, J.P., Garreaud, R., Seibert, J., Vis, M., 2021. Progressive water deficits during multiyear droughts in basins with long hydrological memory in Chile. *Hydrology and Earth System Sciences* 25, 429–446. URL: <https://hess.copernicus.org/articles/25/429/2021/>, doi:10.5194/hess-25-429-2021.
- 550 Bakker, K., 2012. Water Security: Research Challenges and Opportunities. *Science* 337, 914–915. URL: <https://www.science.org/doi/10.1126/science.1226337>, doi:10.1126/science.1226337.
- 551 Barría, P., Sandoval, I.B., Guzman, C., Chadwick, C., Alvarez-Garreton, C., Díaz-Vasconcellos, R., Ocampo-Melgar, A., Fuster, R., 2021. Water allocation under climate change. *Elementa: Science of the Anthropocene* 9, 00131. URL: <https://online.ucpress.edu/elementa/article/9/1/00131/117183/Water-allocation-under-climate-changeA-diagnosis>, doi:10.1525/elementa.2020.00131.
- 552 Beck, H.E., McVicar, T.R., Vergopolan, N., Berg, A., Lutsko, N.J., Dufour, A., Zeng, Z., Jiang, X., van Dijk, A.I.J.M., Miralles, D.G., 2023. High-resolution (1 km) Köppen-Geiger maps for 1901–2099 based on constrained CMIP6 projections. *Scientific Data* 10. URL: <http://dx.doi.org/10.1038/s41597-023-02549-6>, doi:10.1038/s41597-023-02549-6.
- 553 Beguería, S., Vicente-Serrano, S.M., 2023. SPEI: Calculation of the Standardized Precipitation-Evapotranspiration Index. URL: <https://CRAN.R-project.org/package=SPEI>.
- 554 Boisier, J.P., Alvarez-Garreton, C., Cordero, R.R., Damiani, A., Gallardo, L., Garreaud, R.D., Lambert, F., Ramallo, C., Rojas, M., Rondanelli, R., 2018. Anthropogenic drying in central-southern Chile evidenced by long-term observations and climate model simulations. *Elementa* 6, 74. URL: <https://www.elementascience.org/article/10.1525/elementa.328/>, doi:10.1525/elementa.328.
- 555 Calvin, K., Dasgupta, D., Krinner, G., Mukherji, A., Thorne, P.W., Trisos, C., Romero, J., Aldunce, P., Barrett, K., Blanco, G., Cheung, W.W., Connors, S., Denton, F., Dioungue-Niang, A., Dodman, D., Garschagen, M., Geden, O., Hayward, B., Jones, C., Jotzo, F., Krug, T., Lasco, R., Lee, Y.Y., Masson-Delmotte, V., Meinshausen, M., Mintenbeck, K., Mokssit, A., Otto, F.E., Pathak, M., Pirani, A., Poloczanska, E., Pörtner, H.O., Revi, A., Roberts, D.C., Roy, J., Ruane, A.C., Skea, J., Shukla, P.R., Slade, R., Slangen, A., Sokona, Y., Sörensson, A.A., Tignor, M., Van Vuuren, D., Wei, Y.M., Winkler, H., Zhai, P., Zommers, Z., Hourcade, J.C., Johnson, F.X., Pachauri, S., Simpson, N.P., Singh, C., Thomas, A., Totin, E., Arias, P., Bustamante, M., Elgizouli, I., Flato, G., Howden, M., Méndez-Vallejo, C., Pereira, J.J., Pichs-Madruga, R., Rose, S.K., Saheb, Y., Sánchez Rodríguez, R., Ürge Vorsatz, D., Xiao, C., Yassa, N., Alegría, A., Armour, K., Bednar-Friedl, B., Blok, K., Cissé, G., Dentener, F., Eriksen, S., Fischer, E., Garner, G., Guiavarch, C., Haasnoot, M., Hansen, G., Hauser, M., Hawkins, E., Hermans, T., Kopp, R., Leprince-Ringuet, N., Lewis, J., Ley, D., Ludden, C., Niamir, L., Nicholls, Z., Some, S., Szopa, S., Trewin, B., Van Der Wijst, K.I., Winter, G., Witting, M., Birt, A., Ha, M., Romero, J., Kim, J., Haites, E.F., Jung, Y., Stavins, R., Birt, A., Ha, M., Orendain, D.J.A., Ignon, L., Park, S., Park, Y., Reisinger, A., Cammarano, D., Fischlin, A., Fuglestvedt, J.S., Hansen, G., Ludden, C., Masson-Delmotte, V., Matthews, J.R., Mintenbeck, K., Pirani, A., Poloczanska, E., Leprince-Ringuet, N., Péan, C., 2023. IPCC, 2023: Climate Change 2023: Synthesis Report. Contribution of Working Groups I, II and III to the Sixth Assessment Report of the Intergovernmental Panel on Climate Change [Core Writing Team, H. Lee and J. Romero (eds.)]. IPCC, Geneva, Switzerland. Technical Report. Intergovernmental Panel on Climate Change (IPCC). URL: <https://www.ipcc.ch/report/ar6/syr/>.
- 556 Camps-Valls, G., Campos-Taberner, M., Moreno-Martínez, , Walther, S., Duveiller, G., Cescatti, A., Mahecha, M.D., Muñoz-Marí, J., García-Haro, F.J., Guanter, L., Jung, M., Gamon, J.A., Reichstein, M., Running, S.W., 2021. A unified vegetation index for quantifying the terrestrial biosphere. *Science Advances* 7, eabc7447. URL: <https://www.science.org/doi/10.1126/sciadv.abc7447>, doi:10.1126/sciadv.abc7447.
- 557 Chamling, M., Bera, B., 2020. Spatio-temporal Patterns of Land Use/Land Cover Change in the Bhutan–Bengal Foothill Region Between 1987 and 2019: Study Towards Geospatial Applications and Policy Making. *Earth Systems and Environment* 4, 117–130. URL: <http://link.springer.com/10.1007/s41748-020-00150-0>, doi:10.1007/s41748-020-00150-0.
- 558 Chatterjee, S., Desai, A.R., Zhu, J., Townsend, P.A., Huang, J., 2022. Soil moisture as an essential component for delineating and forecasting agricultural rather than meteorological drought. *Remote Sensing of Environment* 269, 112833. URL: <https://linkinghub.elsevier.com/retrieve/pii/S0034425721005538>, doi:10.1016/j.rse.2021.112833.
- 559 Chen, J., Shao, Z., Huang, X., Zhuang, Q., Dang, C., Cai, B., Zheng, X., Ding, Q., 2022. Assessing the impact of drought-land cover change on global vegetation greenness and productivity. *Science of The Total Environment* 852, 158499. URL:

- 607 <https://linkinghub.elsevier.com/retrieve/pii/S004896972205598X>, doi:10.1016/j.scitotenv.2022.158499.
- 608 Cheng, Y., Oehmcke, S., Brandt, M., Rosenthal, L., Das, A., Vrieling, A., Saatchi, S., Wagner, F., Mugabowindekwe, M.,
609 Verbruggen, W., Beier, C., Horion, S., 2024. Scattered tree death contributes to substantial forest loss in California. *Nature
610 Communications* 15, 641. URL: <https://www.nature.com/articles/s41467-024-44991-z>, doi:10.1038/s41467-024-44991-z.
- 611 Crausbay, S.D., Ramirez, A.R., Carter, S.L., Cross, M.S., Hall, K.R., Bathke, D.J., Betancourt, J.L., Colt, S., Cravens, A.E.,
612 Dalton, M.S., Dunham, J.B., Hay, L.E., Hayes, M.J., McEvoy, J., McNutt, C.A., Moritz, M.A., Nislow, K.H., Raheem, N.,
613 Sanford, T., 2017. Defining Ecological Drought for the Twenty-First Century. *Bulletin of the American Meteorological Society*
614 98, 2543–2550. URL: <https://journals.ametsoc.org/view/journals/bams/98/12/bams-d-16-0292.1.xml>, doi:10.1175/BAMS-D-
615 16-0292.1. publisher: American Meteorological Society.
- 616 Dai, M., Huang, S., Huang, Q., Leng, G., Guo, Y., Wang, L., Fang, W., Li, P., Zheng, X., 2020. Assessing agricultural drought
617 risk and its dynamic evolution characteristics. *Agricultural Water Management* 231, 106003. URL: [https://linkinghub.elsevier.com/retrieve/pii/S0378377419316531](https://linkinghub.
618 elsevier.com/retrieve/pii/S0378377419316531), doi:10.1016/j.agwat.2020.106003.
- 619 Didan, K., 2015. MOD13Q1 MODIS/Terra Vegetation Indices 16-Day L3 Global 250m SIN Grid V006. Technical Report.
620 NASA EOSDIS Land Processes DAAC. doi:<http://dx.doi.org/10.5067/MODIS/MOD13Q1.006>.
- 621 Duran-Llacer, I., Munizaga, J., Arumí, J., Ruybal, C., Aguayo, M., Sáez-Carrillo, K., Arriagada, L., Rojas, O., 2020. Lessons
622 to Be Learned: Groundwater Depletion in Chile's Ligua and Petorca Watersheds through an Interdisciplinary Approach.
623 *Water* 12, 2446. URL: <https://www.mdpi.com/2073-4441/12/9/2446>, doi:10.3390/w12092446.
- 624 Echeverría, C., Newton, A., Nahuelhual, L., Coomes, D., Rey-Benayas, J.M., 2012. How landscapes change: Integration of
625 spatial patterns and human processes in temperate landscapes of southern Chile. *Applied Geography* 32, 822–831. URL:
626 <https://linkinghub.elsevier.com/retrieve/pii/S0143622811001676>, doi:10.1016/j.apgeog.2011.08.014.
- 627 FAO, 2022. The State of the World's Forests 2022. FAO. URL: <http://www.fao.org/documents/card/en/c/cb9360en>.
- 628 Farahmand, A., AghaKouchak, A., 2015. A generalized framework for deriving nonparametric standardized drought indicators.
629 *Advances in Water Resources* 76, 140–145. URL: <https://linkinghub.elsevier.com/retrieve/pii/S0309170814002322>, doi:10.
630 1016/j.advwatres.2014.11.012.
- 631 Fathi-Taperasht, A., Shafizadeh-Moghadam, H., Minaei, M., Xu, T., 2022. Influence of drought duration and severity on
632 drought recovery period for different land cover types: evaluation using MODIS-based indices. *Ecological Indicators* 141,
633 109146. URL: <https://linkinghub.elsevier.com/retrieve/pii/S1470160X22006185>, doi:10.1016/j.ecolind.2022.109146.
- 634 Ford, T.W., Otkin, J.A., Quiring, S.M., Lisonbee, J., Woloszyn, M., Wang, J., Zhong, Y., 2023. Flash Drought Indicator
635 Intercomparison in the United States. *Journal of Applied Meteorology and Climatology* 62, 1713–1730. URL: [https://journals.ametsoc.org/view/journals/apme/62/12/JAMC-D-23-0081.1](https://
636 journals.ametsoc.org/view/journals/apme/62/12/JAMC-D-23-0081.1.xml).
- 637 Fuentes, I., Fuster, R., Avilés, D., Vervoort, W., 2021. Water scarcity in central Chile: the effect of climate and land cover
638 changes on hydrologic resources. *Hydrological Sciences Journal* 66, 1028–1044. URL: [https://www.tandfonline.com/doi/full/10.1080/02626667.2021.1903475](https://www.tandfonline.com/doi/
639 full/10.1080/02626667.2021.1903475), doi:10.1080/02626667.2021.1903475.
- 640 Garreaud, R., Alvarez-Garreton, C., Barichivich, J., Boisier, J.P., Christie, D., Galleguillos, M., LeQuesne, C., McPhee, J.,
641 Zambrano-Bigiarini, M., 2017. The 2010–2015 mega drought in Central Chile: Impacts on regional hydroclimate and
642 vegetation. *Hydrology and Earth System Sciences Discussions* 2017, 1–37. URL: [http://www.hydrol-earth-syst-sci-discuss.net/hess-2017-191/](http://www.hydrol-earth-syst-sci-discuss.
643 net/hess-2017-191/), doi:10.5194/hess-2017-191.
- 644 Garreaud, R.D., 2009. The Andes climate and weather. *Advances in Geosciences* 22, 3–11. URL: [https://adgeo.copernicus.org/articles/22/3/2009/](https://adgeo.copernicus.
645 org/articles/22/3/2009/), doi:10.5194/adgeo-22-3-2009.
- 646 Gebrechorkos, S.H., Peng, J., Dyer, E., Miralles, D.G., Vicente-Serrano, S.M., Funk, C., Beck, H.E., Asfaw, D.T., Singer, M.B.,
647 Dadson, S.J., 2023. Global high-resolution drought indices for 1981–2022. *Earth System Science Data* 15, 5449–5466. URL:
648 <https://essd.copernicus.org/articles/15/5449/2023/>, doi:10.5194/essd-15-5449-2023.
- 649 Hao, Z., AghaKouchak, A., 2013. Multivariate Standardized Drought Index: A parametric multi-index model. *Advances in Wa-
650 ter Resources* 57, 12–18. URL: <https://linkinghub.elsevier.com/retrieve/pii/S0309170813000493>, doi:10.1016/j.advwatres.
651 2013.03.009.
- 652 Hargreaves, G.H., 1994. Defining and Using Reference Evapotranspiration. *Journal of Irrigation and Drainage Engineering* 120,
653 1132–1139. URL: <https://ascelibrary.org/doi/10.1061/%28ASCE%290733-9437%281994%29120%3A6%281132%29>, doi:10.
654 1061/(ASCE)0733-9437(1994)120:6(1132).
- 655 Hargreaves, G.H., Samani, Z.A., 1985. Reference crop evapotranspiration from temperature. *Applied engineering in agriculture*
656 1, 96–99.
- 657 Heim, R.R., 2002. A Review of Twentieth-Century Drought Indices Used in the United States. *Bulletin of the American
658 Meteorological Society* 83, 1149–1166. URL: <https://journals.ametsoc.org/doi/10.1175/1520-0477-83.8.1149>, doi:10.1175/
659 1520-0477-83.8.1149.
- 660 Helman, D., Mussery, A., Lensky, I.M., Leu, S., 2014. Detecting changes in biomass productivity in a different land management
661 regimes in drylands using satellite-derived vegetation index. *Soil Use and Management* 30, 32–39. URL: [https://bsssjournals.onlinelibrary.wiley.com/doi/10.1111/sum.12099](https://bsssjournals.
662 onlinelibrary.wiley.com/doi/10.1111/sum.12099), doi:10.1111/sum.12099.
- 663 Hijmans, R.J., 2023. terra: Spatial Data Analysis. URL: <https://CRAN.R-project.org/package=terra>.
- 664 Ho, T.K., 1995. Random decision forests, in: *Proceedings of 3rd international conference on document analysis and recognition*,
665 IEEE. pp. 278–282.
- 666 Hobbins, M.T., Wood, A., McEvoy, D.J., Huntington, J.L., Morton, C., Anderson, M., Hain, C., 2016. The Evaporative Demand
667 Drought Index. Part I: Linking Drought Evolution to Variations in Evaporative Demand. *Journal of Hydrometeorology* 17,
668 1745–1761. URL: <http://journals.ametsoc.org/doi/10.1175/JHM-D-15-0121.1>, doi:10.1175/JHM-D-15-0121.1.
- 669 Homer, C., Dewitz, J., Jin, S., Xian, G., Costello, C., Danielson, P., Gass, L., Funk, M., Wickham, J., Stehman, S., Auch, R.,
670 Riitters, K., 2020. Conterminous United States land cover change patterns 2001–2016 from the 2016 National Land Cover
671 Database. *ISPRS Journal of Photogrammetry and Remote Sensing* 162, 184–199. URL: [20](https://linkinghub.elsevier.com/</p>
</div>
<div data-bbox=)

- retrieve/pii/S0924271620300587, doi:10.1016/j.isprsjprs.2020.02.019.
- Hufkens, K., Stauffer, R., Campitelli, E., 2019. The ecmwfr package: an interface to ECMWF API endpoints. URL: <https://bluegreen-labs.github.io/ecmwfr/>.
- Humphrey, V., Berg, A., Ciais, P., Gentine, P., Jung, M., Reichstein, M., Seneviratne, S.I., Frankenberg, C., 2021. Soil moisture–atmosphere feedback dominates land carbon uptake variability. *Nature* 592, 65–69. URL: <https://www.nature.com/articles/s41586-021-03325-5>, doi:10.1038/s41586-021-03325-5.
- IPCC, 2013. Climate Change 2013: The Physical Science Basis. Contribution of Working Group I to the Fifth Assessment Report of the Intergovernmental Panel on Climate Change. Cambridge University Press, Cambridge, UK; New York, USA. URL: www.climatechange2013.org, doi:10.1017/CBO9781107415324.
- Jiang, W., Wang, L., Feng, L., Zhang, M., Yao, R., 2020. Drought characteristics and its impact on changes in surface vegetation from 1981 to 2015 in the Yangtze River Basin, China. *International Journal of Climatology* 40, 3380–3397. URL: <https://rmets.onlinelibrary.wiley.com/doi/10.1002/joc.6403>, doi:10.1002/joc.6403.
- Kendall, M., 1975. Rank correlation methods (4th ed. 2d impression). Griffin.
- Kogan, F., Guo, W., Yang, W., 2020. Near 40-year drought trend during 1981–2019 earth warming and food security. *Geomatics, Natural Hazards and Risk* 11, 469–490. URL: <https://www.tandfonline.com/doi/full/10.1080/19475705.2020.1730452>, doi:10.1080/19475705.2020.1730452.
- Kuhn, M., Wickham, H., 2020. Tidymodels: a collection of packages for modeling and machine learning using tidyverse principles. URL: <https://www.tidymodels.org>.
- Kunst, J., Zambrano, F., 2023. ODES Estaciones. URL: <https://zenodo.org/record/8189816>.
- Laimighofer, J., Laaha, G., 2022. How standard are standardized drought indices? Uncertainty components for the SPI & SPEI case. *Journal of Hydrology* 613, 128385. URL: <https://linkinghub.elsevier.com/retrieve/pii/S0022169422009544>, doi:10.1016/j.jhydrol.2022.128385.
- Li, H., Choy, S., Zaminpardaz, S., Wang, X., Liang, H., Zhang, K., 2024. Flash drought monitoring using diurnal-provided evaporative demand drought index. *Journal of Hydrology* 633, 130961. URL: <https://linkinghub.elsevier.com/retrieve/pii/S002216942400355X>, doi:10.1016/j.jhydrol.2024.130961.
- Li, W., Migliavacca, M., Forkel, M., Denissen, J.M.C., Reichstein, M., Yang, H., Duveiller, G., Weber, U., Orth, R., 2022. Widespread increasing vegetation sensitivity to soil moisture. *Nature Communications* 13, 3959. URL: <https://www.nature.com/articles/s41467-022-31667-9>, doi:10.1038/s41467-022-31667-9.
- Liu, X., Yu, S., Yang, Z., Dong, J., Peng, J., 2024. The first global multi-timescale daily SPEI dataset from 1982 to 2021. *Scientific Data* 11, 223. URL: <https://www.nature.com/articles/s41597-024-03047-z>, doi:10.1038/s41597-024-03047-z.
- Luebert, F., Pliscott, P., 2022. The vegetation of Chile and the EcoVeg approach in the context of the International Vegetation Classification project. *Vegetation Classification and Survey* 3, 15–28. URL: <https://vcs.pensoft.net/article/67893/>, doi:10.3897/VCS.67893.
- Luyssaert, S., Jammet, M., Stoy, P.C., Estel, S., Pongratz, J., Ceschia, E., Churkina, G., Don, A., Erb, K., Ferlicoq, M., Gielen, B., Grünwald, T., Houghton, R.A., Klumpp, K., Knohl, A., Kolb, T., Kuemmerle, T., Laurila, T., Lohila, A., Loustau, D., McGrath, M.J., Meyfroidt, P., Moors, E.J., Naudts, K., Novick, K., Otto, J., Pilegaard, K., Pio, C.A., Rambal, S., Rebmann, C., Ryder, J., Suyker, A.E., Varlagin, A., Wattenbach, M., Dolman, A.J., 2014. Land management and land-cover change have impacts of similar magnitude on surface temperature. *Nature Climate Change* 4, 389–393. URL: <https://www.nature.com/articles/nclimate2196>, doi:10.1038/nclimate2196.
- Masson-Delmotte, V., P.Z.A.P.S.L.C.C.P.S.B.N.C.Y.C.L.G.M.I.G.M.H.K.L.E.L.J.B.R.M.T.K.M.T.W.O.Y.R.Y.a.B.Z.e., 2021. IPCC, 2021: Climate Change 2021: The Physical Science Basis. Contribution of Working Group I to the Sixth Assessment Report of the Intergovernmental Panel on Climate Change. Technical Report. URL: <https://www.ipcc.ch/>. publication Title: Cambridge University Press. In Press.
- McEvoy, D.J., Huntington, J.L., Hobbins, M.T., Wood, A., Morton, C., Anderson, M., Hain, C., 2016. The Evaporative Demand Drought Index. Part II: CONUS-Wide Assessment against Common Drought Indicators. *Journal of Hydrometeorology* 17, 1763–1779. URL: <http://journals.ametsoc.org/doi/10.1175/JHM-D-15-0122.1>, doi:10.1175/JHM-D-15-0122.1.
- Meroni, M., Rembold, F., Fasbender, D., Vrieling, A., 2017. Evaluation of the Standardized Precipitation Index as an early predictor of seasonal vegetation production anomalies in the Sahel. *Remote Sensing Letters* 8, 301–310. URL: <http://www.tandfonline.com/doi/abs/10.1080/2150704X.2016.1264020>, doi:10.1080/2150704X.2016.1264020.
- Miranda, A., Lara, A., Altamirano, A., Di Bella, C., González, M.E., Julio Camarero, J., 2020. Forest browning trends in response to drought in a highly threatened mediterranean landscape of South America. *Ecological Indicators* 115, 106401. URL: <https://linkinghub.elsevier.com/retrieve/pii/S1470160X20303381>, doi:10.1016/j.ecolind.2020.106401.
- Muñoz, A.A., Klock-Barría, K., Alvarez-Garreton, C., Aguilera-Betti, I., González-Reyes, A., Lastra, J.A., Chávez, R.O., Barría, P., Christie, D., Rojas-Badilla, M., LeQuesne, C., 2020. Water Crisis in Petorca Basin, Chile: The Combined Effects of a Mega-Drought and Water Management. *Water* 12, 648. URL: <https://www.mdpi.com/2073-4441/12/3/648>, doi:10.3390/w12030648.
- Muñoz-Sabater, J., Dutra, E., Agustí-Panareda, A., Albergel, C., Arduini, G., Balsamo, G., Boussetta, S., Choulga, M., Harrigan, S., Hersbach, H., Martens, B., Miralles, D.G., Piles, M., Rodríguez-Fernández, N.J., Zsoter, E., Buontempo, C., Thépaut, J.N., 2021. ERA5-Land: a state-of-the-art global reanalysis dataset for land applications. *Earth System Science Data* 13, 4349–4383. URL: <https://essd.copernicus.org/articles/13/4349/2021/>, doi:10.5194/essd-13-4349-2021.
- Narasimhan, B., Srinivasan, R., 2005. Development and evaluation of Soil Moisture Deficit Index (SMDI) and Evapotranspiration Deficit Index (ETDI) for agricultural drought monitoring. *Agricultural and Forest Meteorology* 133, 69–88. URL: <https://linkinghub.elsevier.com/retrieve/pii/S0168192305001565>, doi:10.1016/j.agrformet.2005.07.012.
- Nicolai-Shaw, N., Zscheischler, J., Hirschi, M., Gudmundsson, L., Seneviratne, S.I., 2017. A drought event composite analysis using satellite remote-sensing based soil moisture. *Remote Sensing of Environment* 203, 216–225. URL: <https://linkinghub>.

- elsevier.com/retrieve/pii/S0034425717302729, doi:10.1016/j.rse.2017.06.014.
- Noguera, I., Vicente-Serrano, S.M., Domínguez-Castro, F., 2022. The Rise of Atmospheric Evaporative Demand Is Increasing Flash Droughts in Spain During the Warm Season. *Geophysical Research Letters* 49, e2021GL097703. URL: <https://agupubs.onlinelibrary.wiley.com/doi/10.1029/2021GL097703>, doi:10.1029/2021GL097703.
- Paruelo, J.M., Texeira, M., Staiano, L., Mastrángelo, M., Amdan, L., Gallego, F., 2016. An integrative index of Ecosystem Services provision based on remotely sensed data. *Ecological Indicators* 71, 145–154. URL: <https://www.sciencedirect.com/science/article/pii/S1470160X16303843>, doi:10.1016/J.ECOLIND.2016.06.054. publisher: Elsevier.
- Pebesma, E., 2018. Simple Features for R: Standardized Support for Spatial Vector Data. *The R Journal* 10, 439–446. URL: <https://doi.org/10.32614/RJ-2018-009>, doi:10.32614/RJ-2018-009.
- Pebesma, E., Bivand, R., 2023. *Spatial Data Science: With applications in R*. Chapman and Hall/CRC, London. URL: <https://r-spatial.org/book/>.
- Peng, D., Zhang, B., Wu, C., Huete, A.R., Gonsamo, A., Lei, L., Ponce-Campos, G.E., Liu, X., Wu, Y., 2017. Country-level net primary production distribution and response to drought and land cover change. *Science of The Total Environment* 574, 65–77. URL: <https://linkinghub.elsevier.com/retrieve/pii/S0048969716319507>, doi:10.1016/j.scitotenv.2016.09.033.
- Pitman, A.J., De Noblet-Ducoudré, N., Avila, F.B., Alexander, L.V., Boisier, J.P., Brovkin, V., Delire, C., Cruz, F., Donat, M.G., Gayler, V., Van Den Hurk, B., Reick, C., Voldoire, A., 2012. Effects of land cover change on temperature and rainfall extremes in multi-model ensemble simulations. *Earth System Dynamics* 3, 213–231. URL: <https://esd.copernicus.org/articles/3/213/2012/>, doi:10.5194/esd-3-213-2012.
- Popová, V., Stepánek, P., Mozný, M., Türkott, L., Soukup, J., 2015. Performance of the standarised precipitation evapotranspiration index at various lags for agricultural drought risk assessment in the {C}zech {R}epublic. *Agricultural and Forest Meteorology* 202, 26–38.
- R Core Team, 2023. R: A Language and Environment for Statistical Computing. R Foundation for Statistical Computing, Vienna, Austria. URL: <https://www.R-project.org/>.
- Rhee, J., Im, J., Carbone, G.J., 2010. Monitoring agricultural drought for arid and humid regions using multi-sensor remote sensing data. *Remote Sensing of Environment* 114, 2875–2887. URL: <http://www.sciencedirect.com/science/article/pii/S003442571000221X>, doi:10.1016/j.rse.2010.07.005.
- Running, S., Zhao, M., 2019. MOD17A3HGF MODIS/Terra Net Primary Production Gap-Filled Yearly L4 Global 500 m SIN Grid V006. URL: <https://lpdaac.usgs.gov/products/mod17a3hgf006/>, doi:10.5067/MODIS/MOD17A3HGF.006.
- Schulz, J.J., Cayuela, L., Echeverria, C., Salas, J., Rey Benayas, J.M., 2010. Monitoring land cover change of the dryland forest landscape of Central Chile (1975–2008). *Applied Geography* 30, 436–447. URL: <https://linkinghub.elsevier.com/retrieve/pii/S0143622809000885>, doi:10.1016/j.apgeog.2009.12.003.
- Sen, P.K., 1968. Estimates of the Regression Coefficient Based on Kendall's Tau. *Journal of the American Statistical Association* 63, 1379–1389. URL: <http://www.tandfonline.com/doi/abs/10.1080/01621459.1968.10480934>, doi:10.1080/01621459.1968.10480934.
- Senf, C., Buras, A., Zang, C.S., Rammig, A., Seidl, R., 2020. Excess forest mortality is consistently linked to drought across Europe. *Nature Communications* 11, 6200. URL: <https://www.nature.com/articles/s41467-020-19924-1>, doi:10.1038/s41467-020-19924-1.
- Slette, I.J., Post, A.K., Awad, M., Even, T., Punzalan, A., Williams, S., Smith, M.D., Knapp, A.K., 2019. How ecologists define drought, and why we should do better. *Global Change Biology* 25, 3193–3200. URL: <https://onlinelibrary.wiley.com/doi/10.1111/gcb.14747>, doi:10.1111/gcb.14747.
- Song, X.P., Hansen, M.C., Stehman, S.V., Potapov, P.V., Tyukavina, A., Vermote, E.F., Townshend, J.R., 2018. Global land change from 1982 to 2016. *Nature* 560, 639–643. URL: <https://www.nature.com/articles/s41586-018-0411-9>, doi:10.1038/s41586-018-0411-9.
- Souza, A.G.S.S., Ribeiro Neto, A., Souza, L.L.D., 2021. Soil moisture-based index for agricultural drought assessment: SMADI application in Pernambuco State-Brazil. *Remote Sensing of Environment* 252, 112124. URL: <https://linkinghub.elsevier.com/retrieve/pii/S0034425720304971>, doi:10.1016/j.rse.2020.112124.
- Taucare, M., Viguier, B., Figueiroa, R., Daniele, L., 2024. The alarming state of Central Chile's groundwater resources: A paradigmatic case of a lasting overexploitation. *Science of The Total Environment* 906, 167723. URL: <https://linkinghub.elsevier.com/retrieve/pii/S0048969723063507>, doi:10.1016/j.scitotenv.2023.167723.
- Tennekes, M., 2018. tmap: Thematic Maps in R. *Journal of Statistical Software* 84, 1–39. doi:10.18637/jss.v084.i06.
- Urrutia-Jalabert, R., González, M.E., González-Reyes, , Lara, A., Garreaud, R., 2018. Climate variability and forest fires in central and south-central Chile. *Ecosphere* 9, e02171. URL: <https://esajournals.onlinelibrary.wiley.com/doi/10.1002/ecs2.2171>, doi:10.1002/ecs2.2171.
- Van Loon, A.F., Gleeson, T., Clark, J., Van Dijk, A.I., Stahl, K., Hannaford, J., Di Baldassarre, G., Teuling, A.J., Tallaksen, L.M., Uijlenhoet, R., Hannah, D.M., Sheffield, J., Svoboda, M., Verbeiren, B., Wagener, T., Rangecroft, S., Wanders, N., Van Lanen, H.A., 2016. Drought in the Anthropocene. *Nature Geoscience* 9, 89–91. doi:10.1038/ngeo2646.
- Van Loon, A.F., Van Huijgevoort, M.H.J., Van Lanen, H.A.J., 2012. Evaluation of drought propagation in an ensemble mean of large-scale hydrological models. *Hydrology and Earth System Sciences* 16, 4057–4078. URL: <https://hess.copernicus.org/articles/16/4057/2012/>, doi:10.5194/hess-16-4057-2012.
- Venegas-González, A., Juñent, F.R., Gutiérrez, A.G., Filho, M.T., 2018. Recent radial growth decline in response to increased drought conditions in the northernmost Nothofagus populations from South America. *Forest Ecology and Management* 409, 94–104. URL: <https://linkinghub.elsevier.com/retrieve/pii/S0378112717313993>, doi:10.1016/j.foreco.2017.11.006.
- Venegas-González, A., Muñoz, A.A., Carpintero-Gibson, S., González-Reyes, A., Schneider, I., Gipolou-Zuñiga, T., Aguilera-Betti, I., Roig, F.A., 2023. Sclerophyllous Forest Tree Growth Under the Influence of a Historic Megadrought in the Mediterranean Ecoregion of Chile. *Ecosystems* 26, 344–361. URL: <https://link.springer.com/10.1007/s10021-022-00760-x>,

- 802 doi:[10.1007/s10021-022-00760-x](https://doi.org/10.1007/s10021-022-00760-x).
- 803 Vicente-Serrano, S.M., Azorin-Molina, C., Sanchez-Lorenzo, A., Revuelto, J., López-Moreno, J.I., González-Hidalgo, J.C.,
 804 Moran-Tejeda, E., Espejo, F., 2014. Reference evapotranspiration variability and trends in Spain, 1961–2011. Global
 805 and Planetary Change 121, 26–40. URL: <https://linkinghub.elsevier.com/retrieve/pii/S0921818114001180>, doi:[10.1016/j.gloplacha.2014.06.005](https://doi.org/10.1016/j.gloplacha.2014.06.005).
- 806 Vicente-Serrano, S.M., Beguería, S., López-Moreno, J.I., 2010. A multiscalar drought index sensitive to global warming: The
 807 standardized precipitation evapotranspiration index. Journal of Climate 23, 1696–1718. URL: <http://dx.doi.org/10.1175/2009JCLI2909.1>, doi:[10.1175/2009JCLI2909.1](https://doi.org/10.1175/2009JCLI2909.1).
- 808 Vicente-Serrano, S.M., Peña-Angulo, D., Beguería, S., Domínguez-Castro, F., Tomás-Burguera, M., Noguera, I., Gimeno-Sotelo,
 809 L., El Kenawy, A., 2022. Global drought trends and future projections. Philosophical Transactions of the Royal Society A:
 810 Mathematical, Physical and Engineering Sciences 380, 20210285. URL: <https://royalsocietypublishing.org/doi/10.1098/rsta.2021.0285>, doi:[10.1098/rsta.2021.0285](https://doi.org/10.1098/rsta.2021.0285).
- 811 Vicente-Serrano, S.M., McVicar, T.R., Miralles, D.G., Yang, Y., Tomas-Burguera, M., 2020. Unraveling the influence of
 812 atmospheric evaporative demand on drought and its response to climate change. WIREs Climate Change 11, e632. URL:
 813 <https://wires.onlinelibrary.wiley.com/doi/10.1002/wcc.632>, doi:[10.1002/wcc.632](https://doi.org/10.1002/wcc.632).
- 814 Wickham, H., Averick, M., Bryan, J., Chang, W., McGowan, L.D., François, R., Grolemund, G., Hayes, A., Henry, L., Hester,
 815 J., Kuhn, M., Pedersen, T.L., Miller, E., Bache, S.M., Müller, K., Ooms, J., Robinson, D., Seidel, D.P., Spinu, V., Takahashi,
 816 K., Vaughan, D., Wilke, C., Woo, K., Yutani, H., 2019. Welcome to the tidyverse. Journal of Open Source Software 4, 1686.
 817 doi:[10.21105/joss.01686](https://doi.org/10.21105/joss.01686).
- 818 Wilhite, D.A., Glantz, M.H., 1985. Understanding: The drought phenomenon: The role of definitions. Water International 10,
 819 111–120. URL: <http://dx.doi.org/10.1080/02508068508686328>, doi:[10.1080/02508068508686328](https://doi.org/10.1080/02508068508686328).
- 820 Wilks, D.S., 2011. Empirical distributions and exploratory data analysis. Statistical Methods in the Atmospheric Sciences 100.
- 821 Winkler, K., Fuchs, R., Rounsevell, M., Herold, M., 2021. Global land use changes are four times greater than previously
 822 estimated. Nature Communications 12, 2501. URL: <https://www.nature.com/articles/s41467-021-22702-2>, doi:[10.1038/s41467-021-22702-2](https://doi.org/10.1038/s41467-021-22702-2).
- 823 WMO, Svoboda, M., Hayes, M., Wood, D.A., 2012. Standardized Precipitation Index User Guide. WMO, Geneva. URL:
 824 http://library.wmo.int/opac/index.php?lvl=notice_display&id=13682. series Title: WMO Publication Title: WMO-No.
 825 1090 © Issue: 1090.
- 826 Wright, M.N., Ziegler, A., 2017. ranger: A Fast Implementation of Random Forests for High Dimensional Data in C++ and
 827 R. Journal of Statistical Software 77, 1–17. doi:[10.18637/jss.v077.i01](https://doi.org/10.18637/jss.v077.i01).
- 828 Wu, C., Zhong, L., Yeh, P.J.F., Gong, Z., Lv, W., Chen, B., Zhou, J., Li, J., Wang, S., 2024. An evaluation framework
 829 for quantifying vegetation loss and recovery in response to meteorological drought based on SPEI and NDVI. Science of
 830 The Total Environment 906, 167632. URL: <https://linkinghub.elsevier.com/retrieve/pii/S0048969723062599>, doi:[10.1016/j.scitotenv.2023.167632](https://doi.org/10.1016/j.scitotenv.2023.167632).
- 831 Xiao, C., Zaehle, S., Yang, H., Wigneron, J.P., Schmullius, C., Bastos, A., 2023. Land cover and management effects on
 832 ecosystem resistance to drought stress. Earth System Dynamics 14, 1211–1237. URL: <https://esd.copernicus.org/articles/14/1211/2023/>, doi:[10.5194/esd-14-1211-2023](https://doi.org/10.5194/esd-14-1211-2023).
- 833 Yang, J., Huang, X., 2021. The 30 m annual land cover dataset and its dynamics in China from 1990 to 2019. Earth System
 834 Science Data 13, 3907–3925. URL: <https://essd.copernicus.org/articles/13/3907/2021/>, doi:[10.5194/essd-13-3907-2021](https://doi.org/10.5194/essd-13-3907-2021).
- 835 Zambrano, F., 2023a. Data of monthly climate variables and drought indices within continental Chile for 1981–2023. URL:
 836 <https://zenodo.org/doi/10.5281/zenodo.10359546>, doi:[10.5281/ZENODO.10359546](https://doi.org/10.5281/ZENODO.10359546).
- 837 Zambrano, F., 2023b. Four decades of satellite data for agricultural drought monitoring throughout the growing season in
 838 Central Chile, in: Vijay P. Singh Deepak Jhajharia, R.M., Kumar, R. (Eds.), Integrated Drought Management, Two Volume
 839 Set. CRC Press, p. 28.
- 840 Zambrano, F., Lillo-Saavedra, M., Verbist, K., Lagos, O., 2016. Sixteen years of agricultural drought assessment of the
 841 biobío region in chile using a 250 m resolution vegetation condition index (VCI). Remote Sensing 8, 1–20. URL: <http://www.mdpi.com/2072-4292/8/6/530>, doi:[10.3390/rs8060530](https://doi.org/10.3390/rs8060530). publisher: Multidisciplinary Digital Publishing Institute.
- 842 Zambrano, F., Vrieling, A., Nelson, A., Meroni, M., Tadesse, T., 2018. Prediction of drought-induced reduction of agricultural
 843 productivity in Chile from MODIS, rainfall estimates, and climate oscillation indices. Remote Sensing of Environment
 844 219, 15–30. URL: <https://www.sciencedirect.com/science/article/pii/S0034425718304541>, doi:[10.1016/j.rse.2018.10.006](https://doi.org/10.1016/j.rse.2018.10.006).
 845 publisher: Elsevier.
- 846 Zhao, Y., Feng, D., Yu, L., Wang, X., Chen, Y., Bai, Y., Hernández, H.J., Galleguillos, M., Estades, C., Biging, G.S., Radke,
 847 J.D., Gong, P., 2016. Detailed dynamic land cover mapping of Chile: Accuracy improvement by integrating multi-temporal
 848 data. Remote Sensing of Environment 183, 170–185. URL: <https://linkinghub.elsevier.com/retrieve/pii/S0034425716302188>,
 849 doi:[10.1016/j.rse.2016.05.016](https://doi.org/10.1016/j.rse.2016.05.016).
- 850 Zhou, K., Li, J., Zhang, T., Kang, A., 2021. The use of combined soil moisture data to characterize agricultural drought
 851 conditions and the relationship among different drought types in China. Agricultural Water Management 243, 106479. URL:
 852 <https://linkinghub.elsevier.com/retrieve/pii/S0378377420305965>, doi:[10.1016/j.agwat.2020.106479](https://doi.org/10.1016/j.agwat.2020.106479).

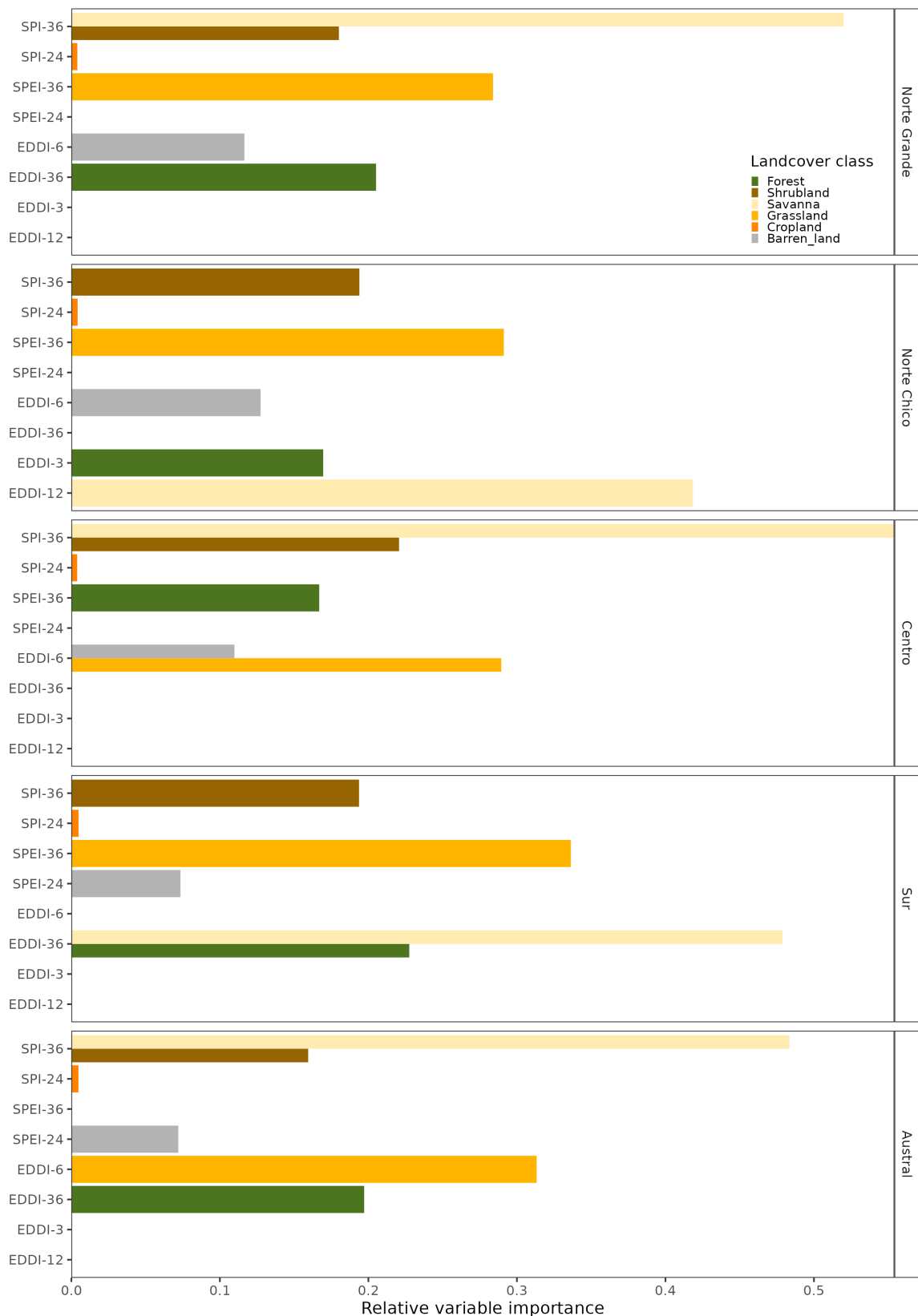


Figure 5: cdcdcdc

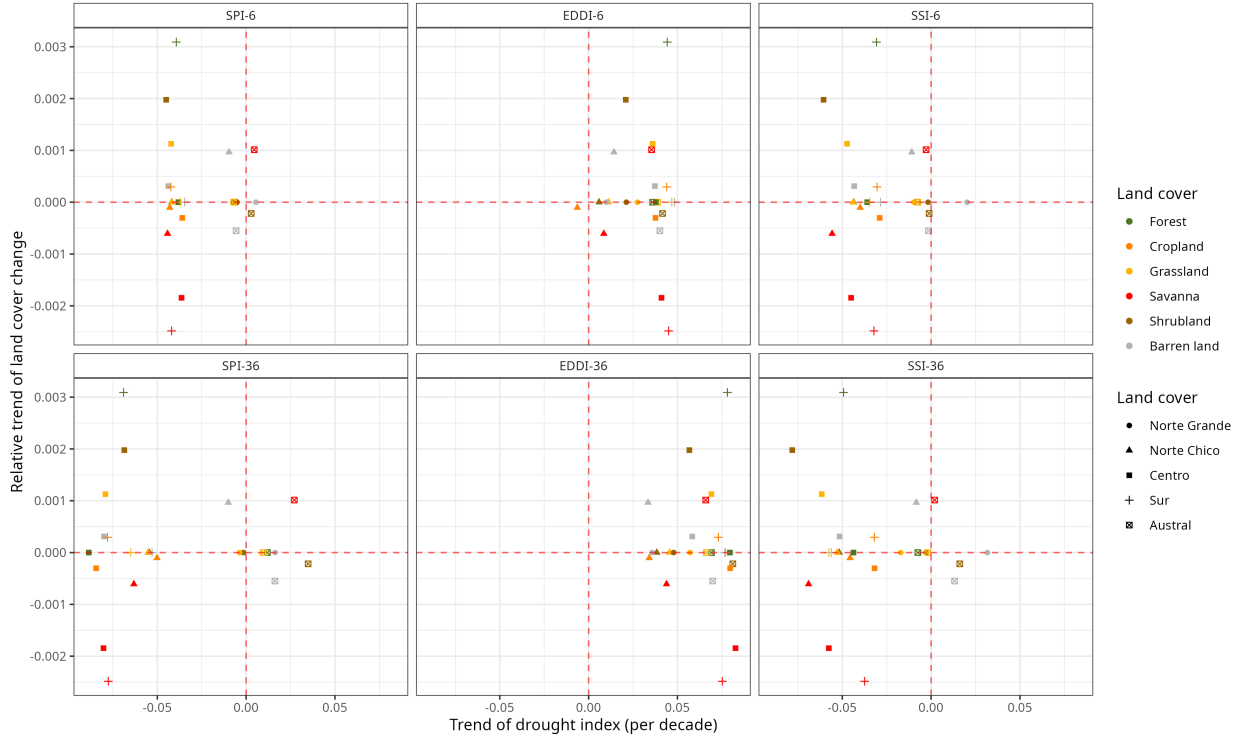


Figure 6: Relationship between the trend in land cover change (y-axis) and the trend in drought indices (x-axis) for the five macrozones. Vertical panels correspond to 1, 3, 6, 12, 24, and 36 months of the time scale by drought index. Horizontal panels show each drought index

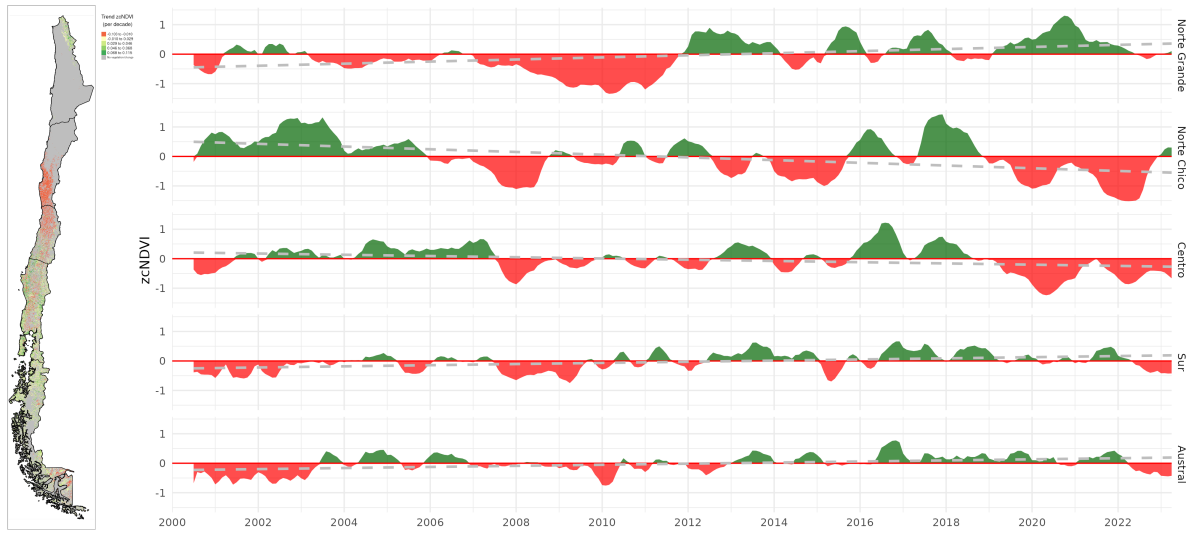


Figure 7: (a) Map of the linear trend of the index zcNDVI for 2000–2023. Greener colors indicate a positive trend; redder colors correspond to a negative trend and a decrease in vegetation productivity. Grey colors indicate either no vegetation or a change in land cover type for 2001–2022. (b) Temporal variation of zcNDVI aggregated at macrozone level within continental Chile. Each horizontal panel corresponds to a macrozone from ‘Norte Grande’ to ‘Austral’.

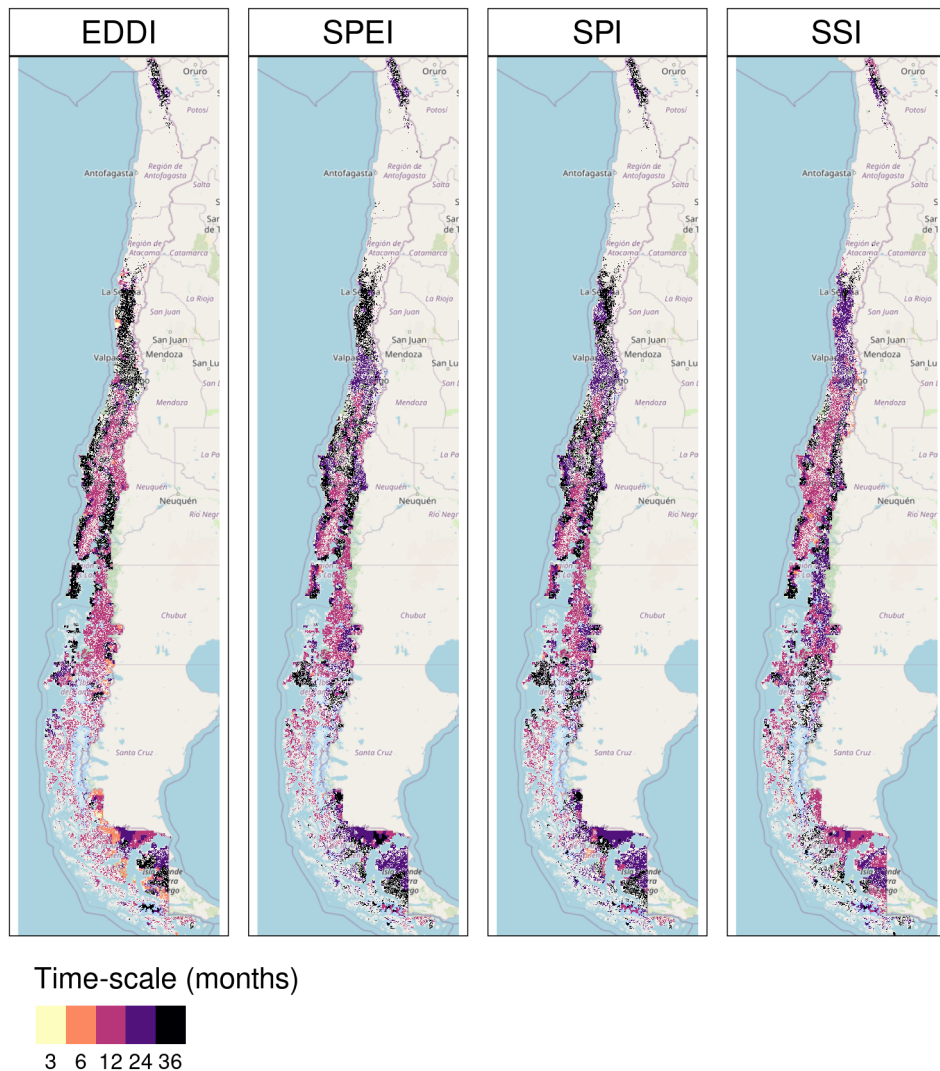


Figure 8: Time scales per drought index that reach the maximum coefficient of determination. White spaces indicate no significant correlation.

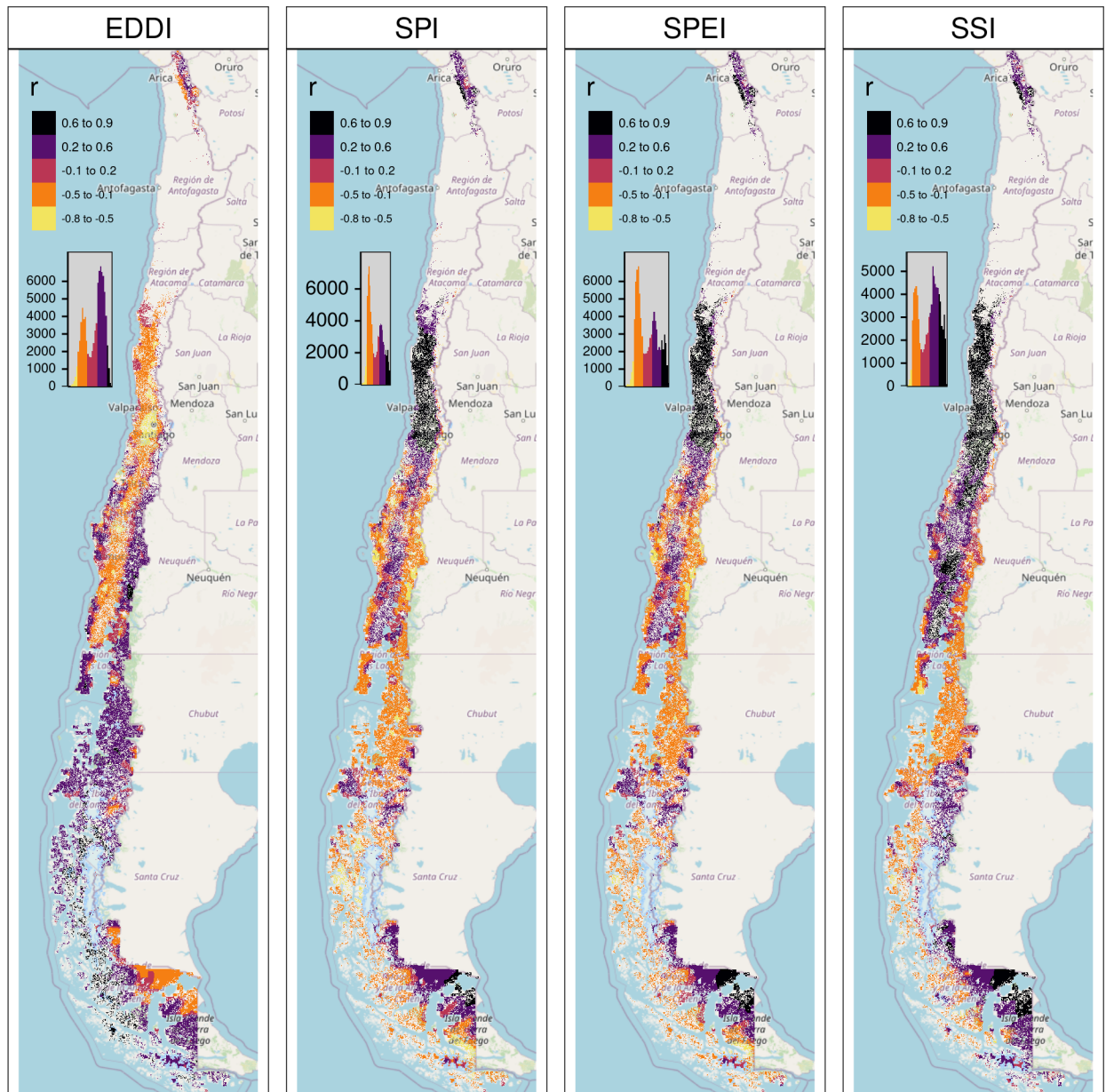


Figure 9: Pearson correlation value for the time scales and drought index that reach the maximum coefficient of determination. White spaces indicate no significant correlation.